Complex sporulation-specific expression of transcription termination factor Rho highlights its involvement in *Bacillus subtilis* cell differentiation

Received for publication, May 27, 2024, and in revised form, October 13, 2024 Published, Papers in Press, October 19, 2024,
https://doi.org/10.1016/j.jbc.2024.107905

Vladimir Bidnenko[1], Arnaud Chastanet[1], Christine Péchoux[2,3], Yulia Redko-Hamel[1], Olivier Pellegrini[4], Sylvain Durand[4], Ciarán Condon[4], Marc Boudvillain[5,6], Matthieu Jules[1], and Elena Bidnenko[1,*]

From the [1]Université Paris-Saclay, INRAE, AgroParisTech, Micalis Institute, Jouy-en-Josas, France; [2]Université Paris-Saclay, INRAE, AgroParisTech, GABI, Jouy-en-Josas, France; [3]MIMA2 Imaging Core Facility, Microscopie et Imagerie des Microorganismes, Animaux et Aliments, INRAE, Jouy-en-Josas, France; [4]Expression Génétique Microbienne, UMR8261 CNRS, Université Paris Cité, Institut de Biologie Physico-Chimique, Paris, France; [5]Centre de Biophysique moléculaire, CNRS UPR4301, Orléans, France; [6]Affiliated with Université d'Orléans, Orléans, France

Reviewed by members of the JBC Editorial Board. Edited by Chris Whitfield

Termination factor Rho, responsible for the main factor–dependent pathway of transcription termination and the major inhibitor of antisense transcription, is an emerging regulator of various physiological processes in microorganisms. In Gram-positive bacterium *Bacillus subtilis*, Rho is involved in the control of cell adaptation to starvation and, in particular, in the control of sporulation, a complex differentiation program leading to the formation of a highly resistant dormant spore. While the initiation of sporulation requires a decrease in Rho protein levels during the transition to stationary phase, the mechanisms regulating the expression of *rho* gene throughout the cell cycle remain largely unknown. Here we show that a drop in the activity of the vegetative SigA-dependent *rho* promoter causes the inhibition of *rho* expression in stationary phase. However, after the initiation of sporulation, *rho* gene is specifically reactivated in two compartments of the sporulating cell using distinct mechanisms. In the mother cell, *rho* expression occurs by read-through transcription initiated at the SigH-dependent promoter of the distal *spo0F* gene. In the forespore, *rho* gene is transcribed from the intrinsic promoter recognized by the alternative sigma factor SigF. These regulatory elements ensure the activity of Rho during sporulation, which appears important for the proper formation of spores. We provide experimental evidence that disruption of the spatiotemporal expression of *rho* during sporulation affects the resistance properties of spores, their morphology, and the ability to return to vegetative growth under favorable growth conditions.

A growing understanding of the importance of transcription termination in the regulation of gene expression in bacteria has stimulated extensive analysis of the proteins that control this universal step in decoding genetic information (1–5). Among them is transcription termination factor Rho, an ATP-dependent RNA helicase-translocase that improves the termination efficiency of many intrinsic terminators and is essential for termination at *bona fide* Rho-dependent terminators (6–10).

Transcriptome analyses of *rho* knockout and conditionally deficient mutants of various bacteria have established the essential role of Rho in controlling pervasive, mainly antisense transcription that originates from cryptic initiation signals or from read-through of transcription terminators (11–14). Thereby Rho directly and indirectly affects gene expression and cellular physiology (14–20). It is notable that in different bacterial species living in diverse habitats, Rho is especially involved in the control of cellular adaptation to stationary phase, including stress survival, cell fate determination, antibiotic sensitivity, host colonization, and virulence (15–19, 21–25). In the Gram-positive bacteria *Bacillus subtilis*, Rho is a part of regulatory network controlling the initiation of sporulation (15, 16). The involvement of Rho in the sporulation process was also demonstrated in *Clostridioides difficile* and *Bacillus thuringiensis* (18, 19).

Sporulation is a complex developmental program that transforms a vegetative bacterial cell into a highly resistant dormant spore, thus ensuring the survival of bacteria under adverse environmental conditions (26–28). A hallmark of sporulation in *B. subtilis* is the asymmetric division of a differentiating cell in two unequal parts: a forespore, which further develops into the spore, and a mother cell, which engulfs the forespore, nourishes it, ensures the synthesis of spore protective layers, and finally lyses to release the mature spore. Proper spore morphogenesis is essential for spore resistance to external damages and its conversion back into a growing cell under favorable conditions through sequential processes of germination and outgrowth (29–35). Sporulation is primarily controlled at the level of transcription initiation by the master regulator Spo0A, whose activity depends on phosphorylation mediated by a multicomponent phosphorelay, the transition phase-specific sigma factor SigH, and a cascade of sigma factors (SigF, SigE, SigG, and SigK) that drives temporally- and spatially-defined, yet interconnected, programs of spore

* For correspondence: Elena Bidnenko, elena.bidnenko@inrae.fr.

morphogenesis. Sporulation is initiated at a threshold level of Spo0A ~ P, which activates the expression of *sigH* and several sporulation genes, including *sigF* and *sigE* encoding the early forespore- and mother cell–specific SigF and SigE factors. Both sigma factors are held inactive until the formation of asymmetric septum, after which SigF is activated the first in the forespore. Consequent activation of SigE in the mother cell depends on SigF activity (36). Compartment-specific programs of gene expression initiated by SigF and SigE are further continued by SigG in the forespore and SigK in the mother cell (37–40). The relevant regulons of each sporulation-specific sigma factor were determined using the combination of experimental and bioinformatics approaches (28, 41–46).

We have previously shown that deletion of the *rho* gene in *B. subtilis* prevents intragenic termination of the *kinB* transcript, which encodes the sensor kinase KinB, one of the main kinases feeding phosphate into the Spo0A phosphorelay. This leads to the increased expression of KinB and, consequently, to rapid accumulation of active Spo0A ~ P to a threshold level that triggers sporulation. Thus, Rho inactivation stimulates sporulation in *B. subtilis* (15). Conversely, maintaining *rho* expression at a stably elevated level throughout *B. subtilis* exponential growth and stationary phase prevents the activation of Spo0A and, additionally, inhibits some late sporulation events, thus blocking the formation of spores (16).

Comparative transcriptome and proteome analyses have revealed a decrease in the levels of *rho* mRNA and Rho protein during the transition to stationary phase in WT *B. subtilis* cells (11, 15, 16). Considering that Rho negatively affected sporulation in our analyses, a decrease in Rho levels appears necessary for both initiation and implementation of the sporulation program. This in turn suggests that *rho* expression during *B. subtilis* growth and stationary phase is subject to reliable and timely regulation.

The only mechanism known to date for regulating *rho* expression is transcriptional attenuation at the Rho-dependent terminator(s) located within the leader region of the *rho* transcript and consequent premature transcription termination (47). Similar to *B. subtilis*, transcription of the *rho* gene was shown to be autogenously regulated in *Escherichia coli*, *Salmonella*, and *Caulobacter crescentus* (48–51). In *Salmonella*, *rho* autoregulation is counteracted by the small noncoding RNA SraL, which prevents the Rho-mediated termination by directly binding the 5′-UTR of *rho* mRNA (51).

In the present study, we aimed to gain further insights into *rho* regulation in *B. subtilis* by analyzing the kinetics of *rho* expression at various stages of cellular growth and differentiation. Quite unexpectedly, we found that the expression of the *rho* gene is specifically induced early during sporulation. This finding has focused our subsequent analysis on understanding the mechanism of the sporulation-specific expression of *rho*. We describe two distinct mechanisms controlling *rho* expression in each compartment of the sporulating cells: read-through transcription from the upstream SigH-dependent promoter in the mother cell and a genuine SigF-dependent *rho* promoter active in the forespore. We provide evidence that altering the spatiotemporal expression of *rho* affects spore resistance properties and morphology. Moreover, spores formed in the absence of Rho are impaired in their ability to revive under favorable growth conditions, exhibiting an accelerated germination and a slow outgrowth. We show that the natural rate of spore outgrowth depends on the *rho* expression both during spore formation and after spore germination.

Results

Rho expression is specifically induced during sporulation

To analyze a real-time expression of the *rho* gene, we constructed a reporter system, in which the luciferase gene *luc* of firefly *Photinus pyralis* was fused to the *rho* promoter (P_{rho}) at the position of the *rho* start codon. The P_{rho}-*luc* fusion was similarly located in the *rho* locus of the chromosome in the WT *B. subtilis* strain BSB1 (hereafter WT) and the *rho* deletion mutant (Δ*rho*) (15). The WT strain kept an active *rho* gene due to DNA duplication within the *rho* locus during the construction. By comparing luciferase activity in WT and Δ*rho* strains under different growth conditions, we sought to assess Rho autoregulation and possibly identify other regulatory factors.

In WT cells grown in rich LB medium, the expression of *rho* was mainly limited to the exponential growth phase, characterized by two peaks of luciferase activity at A_{600} ~0.15 and ~0.4 (Fig. 1*A*). In stationary phase, *rho* expression remained at a basal level. A low-level expression of *rho* and its down-regulation during the transition to stationary phase were reported previously (11, 15, 16, 47). The inactivation of Rho in Δ*rho* cells did not alter the kinetics of P_{rho}-*luc* activity, but rather increased its level approximately threefold, suggesting a loss of the *rho* autoregulation (Fig. 1*A*).

WT cells grown in the sporulation-promoting Difco Sporulation Medium (DSM) showed different *rho* expression kinetics, characterized by an additional peak of luciferase activity in stationary phase (Fig. 1*B*). The reactivation of *rho* expression coincided with the induction of the sporulation-specific *spoIIAA-AB-sigF* operon, monitored in a separate strain using the $P_{spoIIAA}$-*luc* transcriptional fusion (Fig. 1*B*), (15). The similarity in timing suggested that *rho* expression during stationary phase in DSM might be linked to sporulation.

In Δ*rho* cells grown in DSM, luciferase activity increased ~7-fold compared to WT cells during exponential growth, but only ~1.5-fold in stationary phase. This suggests that *rho* expression is not significantly autoregulated in stationary phase. However, the stationary phase-specific expression of *rho* was activated considerably earlier in Δ*rho* than in WT cells (Fig. 1*C*). This effect was reminiscent of the accelerated expression of *spo0A* gene in the sporulating Δ*rho* cells caused by the up-regulation of the Spo0A phosphorelay (15). Therefore, we compared the expression of *rho* and *spo0A* genes in WT and Δ*rho* cells grown in DSM using the P_{rho}-*luc* and P_{spo0A}-*luc* fusions (15, 52). In both strains, luciferase expression from P_{rho}-*luc* in stationary phase followed P_{spo0A}-*luc* and, in Δ*rho* cells, the maximal activity of two fusions was reached ~1.5 h earlier than in WT (Fig. 1*D*). This observation

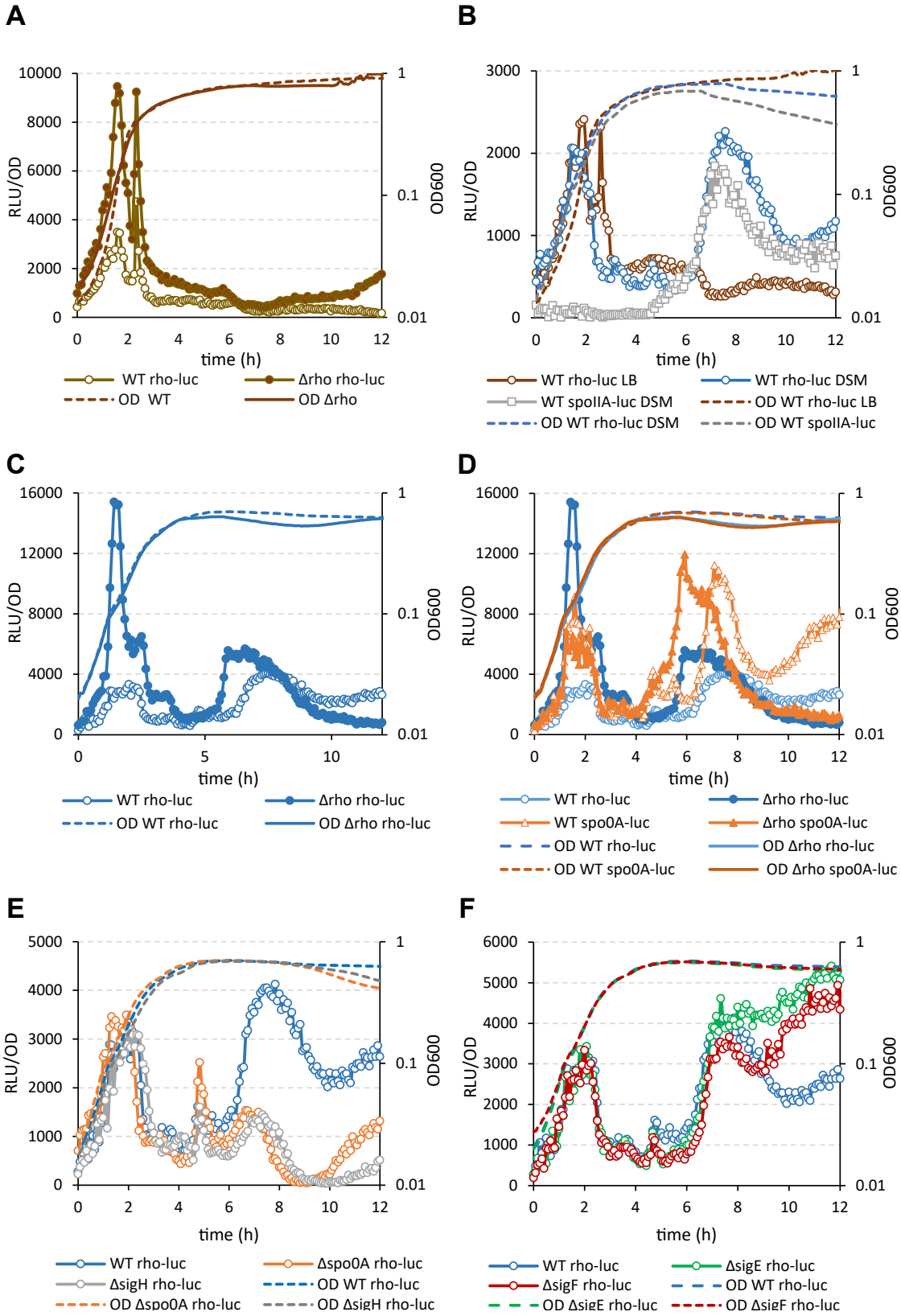

Figure 1. Rho is specifically expressed during *Bacillus subtilis* sporulation. *A*, Rho expression in vegetative cells is limited to the exponential growth phase and autoregulated. Kinetics of luciferase activity in *B. subtilis* WT P_{rho}-*luc* (empty circles) and Δ*rho* P_{rho}-*luc* (filled-in circles) cells grown in rich medium LB. In this and other panels, the plain dotted and solid lines represent growth curves of the Rho-proficient strains and *rho*-deletion mutant (Δ*rho*), respectively, measured by A_{600}. *B*, in the sporulation-inducing conditions, *rho* expression is additionally activated in stationary phase. Comparative analysis of the luciferase activity in WT P_{rho}-*luc* cells grown in LB (*brown* circles) and in sporulation medium DSM (*blue* circles). Activation of luciferase expression from the early sporulation promoter *spoIIA* in the control WT P_{spoIIA}-*luc* cells grown in DSM (*gray* squares) marks the initiation of sporulation. *C*, in the sporulation-inducing conditions, the autoregulation of Rho is weakened in stationary phase. Kinetics of luciferase activity in *B. subtilis* WT P_{rho}-*luc* (empty

additionally argued for the sporulation-specific expression of *rho* as a function of Spo0A ∼ P activity.

To get more insights into the sporulation-specific expression of *rho*, we analyzed the activity of P_{rho}-*luc* in *B. subtilis* sporulation mutants. The mutations *spo0A* and *sigH*, which block the initiation of sporulation, did not affect P_{rho}-*luc* activity during exponential growth in DSM, but severely inhibited it in stationary phase (Fig. 1*E*). This observation confirmed that *rho* expression in stationary phase depends on sporulation-specific factors. However, there were no significant changes in the luciferase activity in Δ*sigF* P_{rho}-*luc* and Δ*sigE* P_{rho}-*luc* mutants suggesting that *rho* can be expressed in both compartments of sporulating cells (Fig. 1*F*). Considering that the known SigA-controlled P_{rho} promoter is mainly active during exponential growth (Fig. 1*A*), we sought for additional regulatory factors of *rho* expression during sporulation.

Sporulation-specific expression of rho *is partially dependent on the read-through transcription from the upstream SigH-controlled promoter*

The *rho* gene is transcribed from the cognate P_{rho} promoter together with the upstream non-coding S1436 element and the downstream *rpmE* gene in a transcript of ∼1.9 kb (7, 11, 47). Additionally, genome-wide transcriptome analyses have revealed several longer read-through transcripts at the *rho* locus, which initiate at the upstream *spo0F* and *fbaA-ywjH* promoters and bypass the intrinsic terminators of the *ywjH* and *glpX* genes (10, 11), (Fig. 2*A*).

We asked whether read-through transcription could play a role in the expression of *rho*, in particular during sporulation, as *spo0F* gene is known to be transcribed from alternative SigA- and SigH-dependent promoters, with the latter also being regulated by Spo0A ∼ P (53–56). To this end, we sought to enhance transcription termination upstream of the *rho* gene and inserted a DNA fragment containing three intrinsic transcription terminators after the stop codon of the *glpX* gene (hereafter 3Ter; Fig. 2*B*) (15, 57). To assess read-through transcription at the *rho* locus and the termination efficiency of the 3Ter insertion, we analyzed *rho*-specific transcripts in WT, Δ*sigH* and 3TER mutant cells by Northern blot (Fig. 2*C*). Cells were grown in DSM and sampled during exponential growth (A_{600} 0.5), transition phase (A_{600} 1.0) and 1.5 h later in stationary phase (A_{600} 1.8).

The major *rho*-specific RNA detected in all strains corresponded in size to the 1.9 kb *rho-rpmE* mRNA (Fig. 2*C*). In addition to this transcript, the WT and Δ*sigH* mutant cells contained several larger *rho*-specific RNA species (Fig. 2*C*). Notably, none of these large *rho*-specific transcripts were detectable in 3TER cells, indicating that they originate from upstream of the inserted terminators (Fig. 2*C*). Moreover, during transition to stationary phase, the large *rho*-specific RNAs accumulated in WT cells, but gradually disappeared in Δ*sigH* mutant, in accordance with the dependence of *spo0F* transcription in stationary phase on SigH activity (Fig. 2*C*). These observations attested to an intensive read-through transcription of the *rho* gene mainly driven, in stationary phase, by the SigH-dependent *spo0F* promoter. To assess the role of the read-through transcription in *rho* expression, we inserted 3Ter into the chromosome of WT P_{rho}-*luc* strain at the location shown in Fig. 2*B*. The luciferase activity in the resulting 3TER P_{rho}-*luc* cells grown in DSM specifically decreased in stationary phase compared to WT P_{rho}-*luc* cells (Fig. 2*D*). We concluded that the read-through transcription from the upstream promoter accounts for at least half of the *rho* expression level during sporulation.

Sporulation-specific expression of rho *is compartmentalized and requires SigF activity in the forespores*

Northern analysis also provided information about the cognate *rho* transcription. The levels of the 1.9 kb *rho-rpmE* mRNA (hereafter *rho* transcript) decreased in the stationary WT cells, in line with the down-regulation of the SigA-dependent P_{rho} at this stage (Fig. 2*C*). Interestingly, this effect was more pronounced in Δ*sigH* mutant cells, in which *rho* transcript became barely detectable in stationary phase (Fig. 2*C*). However, the abundance of *rho* transcript was independent of read-through transcription, as it remained high in the stationary 3TER cells (Fig. 2*C*). We suggested that the difference in the *rho* transcription levels in the stationary Δ*sigH* and 3TER cells could be related to the inhibition of sporulation in the former. To test this hypothesis, we rendered 3TER cells sporulation-deficient by mutating SigF factor, which is the next after SigH in the regulatory cascade of sporulation. The abundance of *rho* transcript in 3TER Δ*sigF* mutant cells in stationary phase considerably decreased compared to 3TER cells, to a level similar to Δ*sigH* mutant (Fig. 2*C*). Following this observation, we tested whether the expression of *rho* in the absence of read-through transcription (Fig. 2*D*) depends on sporulation by using the sporulation-deficient derivatives of 3TER P_{rho}-*luc* strain. Indeed, the residual luminescence in the stationary 3TER P_{rho}-*luc* cells was blocked by *spo0A* and *sigH* inactivation (Fig. 2*E*) and partially inhibited by *sigF* deletion, while Δ*sigE* mutation had no effect (Fig. 2*F*). We concluded that, in addition to the read-through

blue circles) and Δ*rho* P_{rho}-*luc* (filled-in *blue* circles) cells grown in sporulation medium DSM. *D*, Rho expression in the sporulation-inducing conditions correlates with the activation of Spo0A. Comparative analysis of luciferase expression from P_{rho}-*luc* (*blue* circles) and P_{spo0A}-*luc* (*orange* triangles) transcriptional fusions in WT (empty symbols) and Δ*rho* (filled-in symbols) cells grown in DSM. *E* and *F*, Rho expression in stationary phase depends on the initiation of sporulation. Kinetics of luciferase expression from P_{rho}-*luc* transcriptional fusions in WT cells (*blue* circles) and the sporulation mutants (*E*): Δ*spo0A* (*orange* circles) and Δ*sigH* (*gray* circles); and (*F*): Δ*sigF* (*red* circles) and Δ*sigE* (*green* circles). Measurements were taken every 5 min after cells inoculation in media at optical density A_{600} ∼0.025 (time point 0). For each strain, plotted are the mean values of luminescence readings corrected for OD from four independent cultures analyzed simultaneously. Each panel presents the simultaneously collected data. The data in (*C*) and (*D*) and in (*E*) and (*F*) were obtained in two independent experiments. Each strain and growth condition was tested at least three times. The results from the representative experiment are presented.

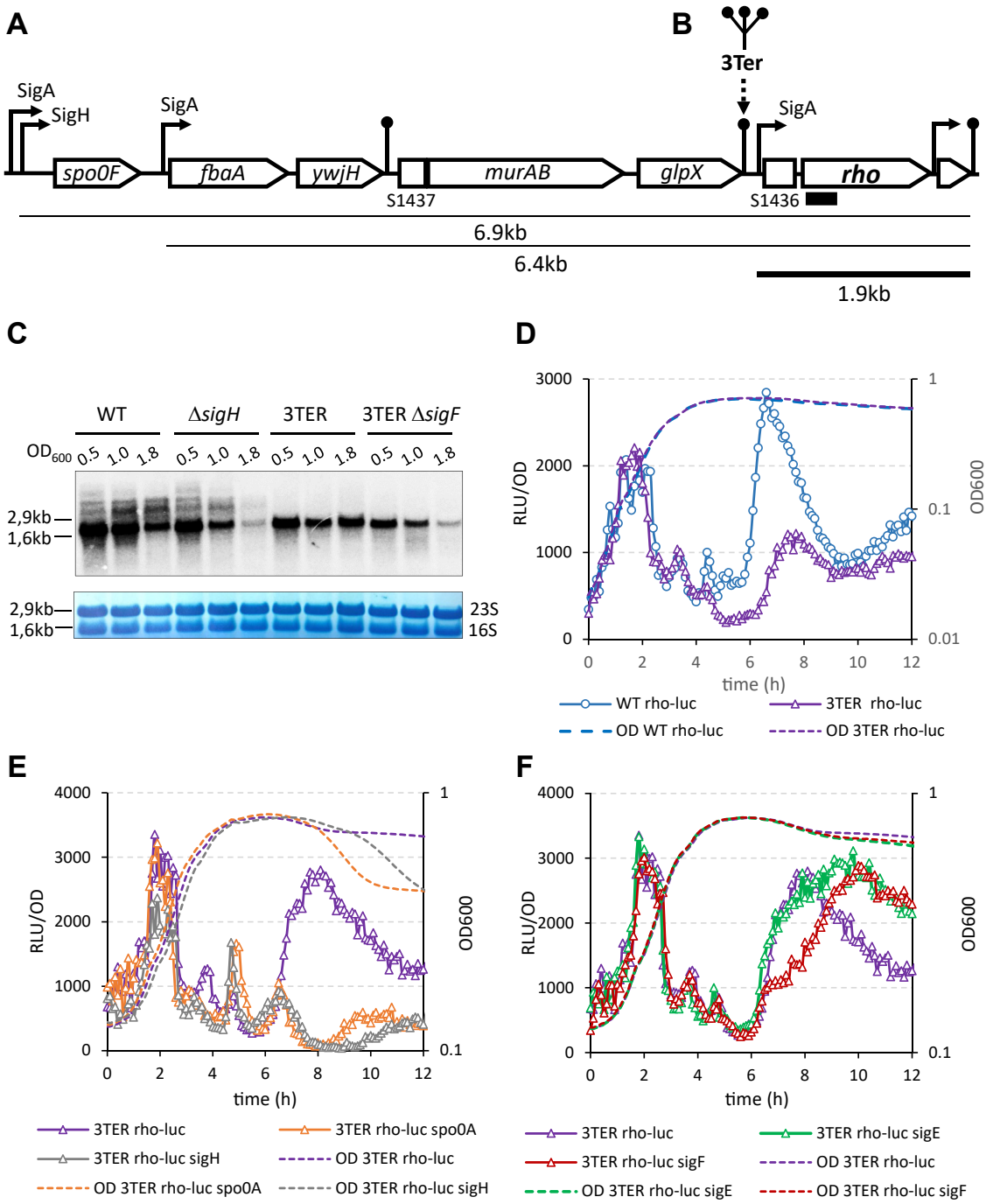

Figure 2. Role of the read-through transcription in the *rho* expression during sporulation. *A*, schematic representation of gene organization and transcription within the *rho* locus of *B. subtilis* chromosome. Arrow-shaped and flat rectangles indicate protein-coding genes and noncoding RNA S-segments (11), respectively. Curved arrow-ended lines represent promoters; their regulatory sigma factors are indicated. Straight dot-ended lines represent intrinsic terminators. The underlying lines indicate the transcripts of the *rho* gene, which were identified in (11); the transcript initiated at the known *rho* promoter is bolded. The approximate size of the transcripts is shown. Small *black* rectangle schematizes the 5′ *rho*-specific riboprobe used in the Northern blot. *B*, cartoon of the insertion of three intrinsic terminators at the end of *glpX* gene in the 3TER strain. *C*, Northern blot analysis of the *rho*-specific transcripts in the WT and the mutant Δ*sigH*, 3TER, and 3TER Δ*sigF* strains during sporulation. Cells were grown in DSM and sampled during exponential growth (A_{600} 0.5), the transition to stationary phase (A_{600} 1.0), and in stationary phase (A_{600} 1.8). Total RNA was extracted, processed, and hybridized with the *rho*-specific riboprobe as described in Experimental procedures. *Upper panel*. The *rho*-specific transcripts visualized by Northern blotting. The lines relate the position of the ribosomal 16S and 23S RNAs visualized by staining of the membrane with 0.2% methylene blue (*bottom panel*). The approximate size of the ribosomal RNAs is indicated. *Bottom panel*. Staining of the ribosomal 16S and 23S RNAs with methylene *blue* allows controlling the equilibrium of the loaded RNA samples and their transfer onto membrane. *D*, suppression of the read-through transcription inhibits *rho* expression in stationary phase. Kinetics of luciferase activity in *B. subtilis* WT P_{rho}-*luc* (*blue circles*) and 3TER P_{rho}-*luc* (*violet triangles*) cells grown in the sporulation-inducing DSM. *E* and *F*, in the absence of read-through transcription, the residual expression of *rho* in stationary phase is sporulation-dependent. Kinetics of luciferase activity in 3TER P_{rho}-*luc* strain (*violet triangles*) and its sporulation mutants (*E*): Δ*spo0A* (*orange triangles*) and Δ*sigH* (*gray triangles*); and (*F*): Δ*sigF* (*red triangles*) and Δ*sigE* (*green triangles*) grown in DSM. The data in (*E*) and (*F*) were obtained in the same experiment and are independent from (*D*). The data were collected and processed as described in Fig. 1. The experiments were reproduced at least three times. The results from the representative experiment are presented.

transcription, *rho* expression during sporulation requires some factor(s) likely dependent on SigF.

SigF is primarily associated with the forespore, but also determines activation of SigE in the mother cell. This led us to investigate potential compartmentalization of *rho* expression during sporulation. To this end, we constructed a P_{rho}-*gfp* fusion expressing green fluorescent protein GFP at the *rho* chromosomal locus of WT cells. Fluorescence microscopy of WT P_{rho}-*gfp* cells sporulating in DSM revealed an increase of fluorescence intensity in the forespores immediately after asymmetric division (Figs. S1 and S3). Following this observation, we analyzed the activity of P_{rho}-*gfp* fusion in Δ*sigF* and Δ*sigE* mutant cells. Inactivation of *sigF* or *sigE* determines a similar disporic phenotype characterized by the formation of asymmetric septa at both poles of sporulating cells (58–61). Such disporic cells were readily observed in Δ*sigF* P_{rho}-*gfp* and Δ*sigE* P_{rho}-*gfp* sporulating cultures, along with cells containing one septum. Both Δ*sigF* and Δ*sigE* mutants maintained a GFP signal in the mother cells at a level similar to that of WT, indicating that *rho* expression in this compartment is SigE-independent (Fig. 3). In contrast, while the forespore-like structures in Δ*sigE* mutant showed high fluorescence levels like the WT forespores, their brightness was significantly diminished in Δ*sigF* mutant (Fig. 3). Together with the results from Fig. 2*C*, this observation indicated that *rho* is expressed in the forespores from a promoter that locates in the *glpX-rho* intergenic region and depends, directly or indirectly, on SigF.

The 5′-UTR of rho *contains a genuine SigF-dependent promoter active in forespores*

Previous analyses have identified a *rho* promoter that matches the SigA-binding sequence consensus ($^{SigA}P_{rho}$) 293 to 320 bp upstream of the *rho* start codon (7, 48), (Fig. 4*A*). Recent reassessment of *B. subtilis* promoters using the unsupervised sequence clustering algorithm has classified $^{SigA}P_{rho}$ to the M16 cluster of SigA-dependent promoters, characterized by an extended 3′-terminal G-rich −10 box and a variable −35 box with the conserved TTG stretch (11), (Fig. 4*B*). Looking for alternative *rho* expression signals, we analyzed the *glpX-rho* intergenic region for the presence of the SigF-binding consensus −35 (GYATA) and −10 (GGnnA-nAHTR) sequences, where Y is C or T; H is A or C or T; R is A or G; and n is any nucleotide (44). Such features were found within the $^{SigA}P_{rho}$ sequence itself (Fig. 4*C*). Overlapping the −10 box of $^{SigA}P_{rho}$, we identified GGTAAAAATA sequence perfectly matching the SigF −10 consensus and, 14 bp upstream, a 5-nucleotide GAATA sequence differing from the SigF −35 consensus by one nucleotide. Of note, the same −35 sequence is present in the SigF-regulated promoters of *yuiC*, *yabT*, *yjbA*, *ypfB* and *ythC* genes (44). Moreover, the 14-bp spacer between the −35 and −10 sequences is highly A/T-rich, characteristic of most SigF-dependent promoters (44).

To prove that the identified sequences constitute a novel SigF-dependent *rho* promoter (hereafter $^{SigF}P_{rho}$), we proceeded to site-directed mutagenesis of the P_{rho}-*gfp* fusion, anticipating that altering the SigF-binding sequences would specifically affect GFP expression in the forespores. Because of

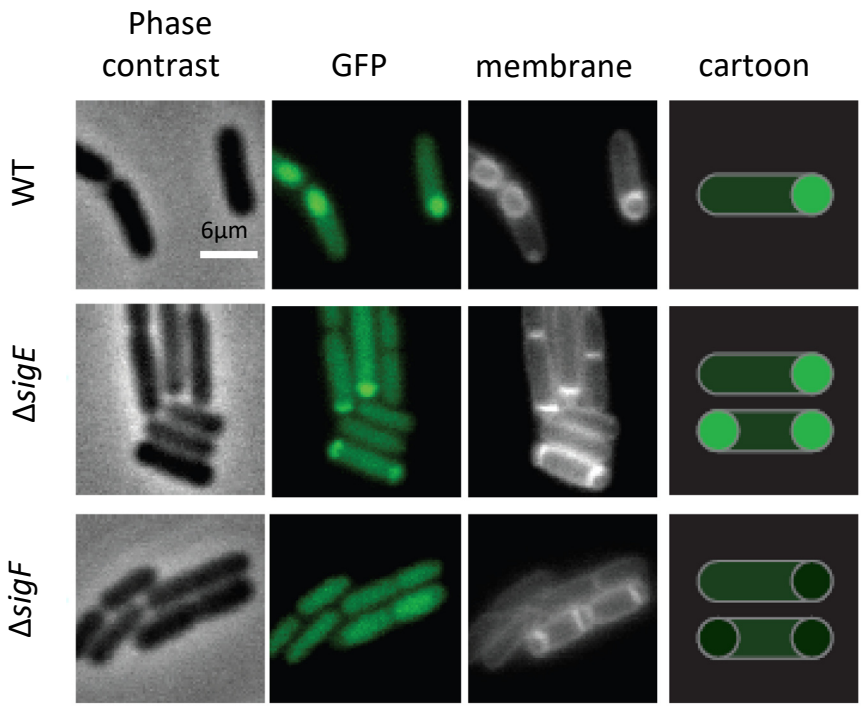

Figure 3. The expression of *rho* in the forespore compartment of sporangium depends on Sigma F. The WT P_{rho}-gfp strain and its ΔsigF and ΔsigE mutant derivatives were induced for sporulation by the resuspension method as described in Experimental procedures. Cells were sampled 3 hours after resuspension in the nutrient-poor SM medium and observed by phase contrast microscopy and by epifluorescence illumination of GFP or membrane-affine dye in two independent replicas. The right-hand cartoon depicts spatial GFP-mediated fluorescence in cells with asymmetric septa.

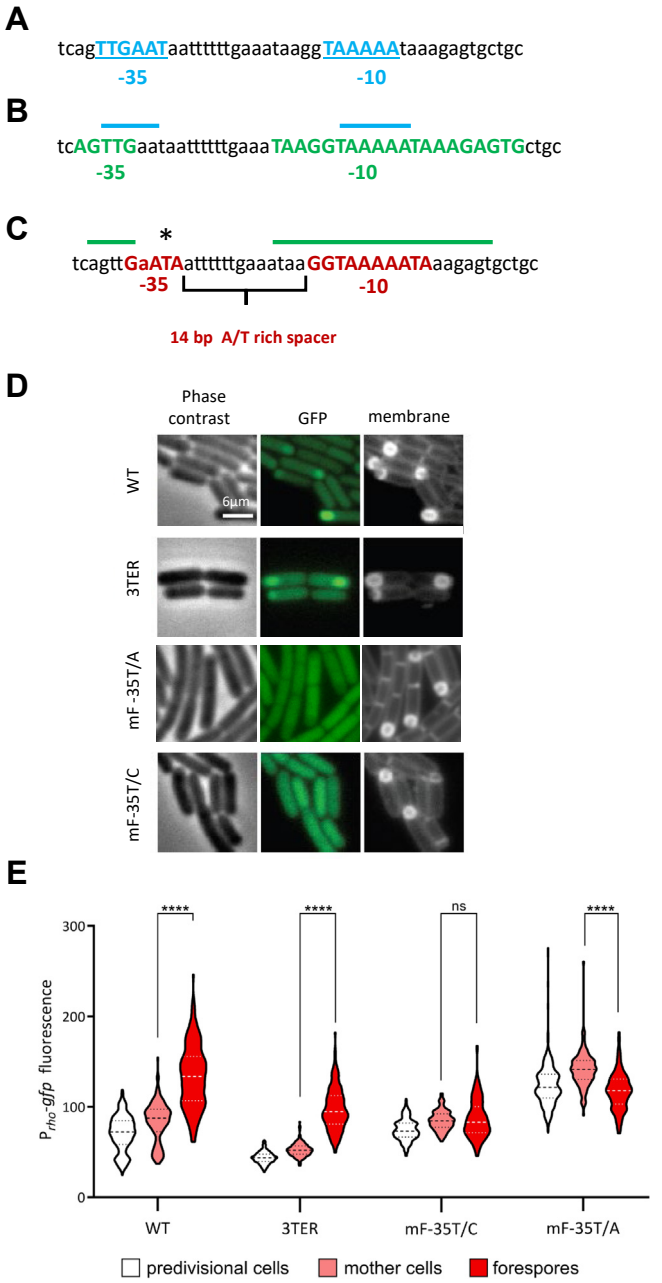

Figure 4. Forespore-specific expression of *rho* depends on the activity of a genuine SigF-dependent promoter. *A* and *B*, sequence and structural elements of the SigA-dependent *rho* promoter reported by: (47) in (*A*) and (11) in (*B*). The −35 and −10 boxes are bolded and colored in *blue* (*A*) and *green* (*B*). In (*B*), the *upper blue* lines indicate the relative position of the *rho* promoter identified by (47). *C*, sequence and structural elements (bolded and colored in *red*) of putative SigF-dependent *rho* promoter identified in this analysis as matching consensus sequences recognized by SigF-containing RNA polymerase (44). The *upper green* lines indicate the relative position of the SigA-dependent *rho* promoter identified by (11). The asterisk indicates a conserved thymine nucleotide in the −35 sequence of the SigF-dependent promoter subjected to mutagenesis. *D* and *E*, mutations of the SigF-dependent *rho* promoter specifically inhibit *rho* expression in the forespores. The WT and 3TER cells bearing the nonmodified P_{rho}-*gfp* fusion and WT P_{rho}-*gfp* cells containing the indicated single-nucleotide mutations of putative SigF-dependent *rho* promoter were induced for sporulation and analyzed for GFP-mediated fluorescence as described in Experimental procedures and Fig. 3. *D*, Micrographs of typical cells observed by phase contrast, epifluorescence illumination of GFP, or membrane-affine dye. *E*, average fluorescence intensities, determined in predivisional cells (*white*) and the mother cell (*rose*) and the forespore (*red*) compartments of sporangia in each strain, are displayed as violin plots. Means and quartiles are represented as *dashed* and *dotted* lines, respectively. N > 100, per strain and per replica. Displayed is a representative experiment from two independent replica. The statistical significance was estimated by a two-tailed *t* test. *p*-values are displayed as follows: **** = $p < 0.0001$; ns = $p > 0$.

a strong overlap between the −10 sequences of $^{SigA}P_{rho}$ and putative $^{SigF}P_{rho}$, we targeted the −35 GAATA sequence of the latter and replaced the invariant T nucleotide (44, 62) with A (*mF-35T/A* P_{rho}-*gfp*) or C (*mF-35T/C* P_{rho}-*gfp*) (Fig. 4*C*). Next, we compared the activity of the mutant fusions with the original one (WT P_{rho}-*gfp*) and the one preceded by the three transcriptional terminators (3TER P_{rho}-*gfp*). Cells were induced to sporulate by the resuspension method and fluorescence levels in pre-divisional cells and two compartments of sporangia were quantified at the time of a maximal SigF activity. As we observed earlier (Fig. 3), the sporulating WT P_{rho}-*gfp* cells showed a higher level of fluorescence in the forespores than in the mother cells; in the latter, *gfp* expression appeared similar to pre-divisional cells confirming that *rho* expression in the mother cell is SigE-independent (Fig. 4, *D* and *E*). A similar pattern of brighter forespores was observed in 3TER P_{rho}-*gfp* cells, even though the fluorescence was globally lower probably due to the inhibition of read-through transcription (Fig. 4, *D* and *E*).

In contrast, and as expected, both the *mF-35T/A* and *mF-35T/C* mutations of P_{rho}-*gfp* specifically inhibited the burst of fluorescence in the forespores, similarly to the *sigF* mutation (Figs. 4, *D* and *E* and 3). At present, it is unclear why *mF-35T/A* P_{rho}-*gfp* mutant strain displayed a higher basal fluorescence (Fig. 4*E*). Nevertheless, these results clearly indicate that the forespore-specific expression of *rho* depends on the alternative promoter $^{SigF}P_{rho}$. This conclusion was further supported by the analysis of the mutated P_{rho}-*luc* fusion: both *mF-35T/A* and *mF-35T/C* point mutations efficiently inhibited sporulation-specific luciferase activity in 3TER cells (Fig. S2).

Differential expression of Rho affects spore properties and morphology

The revealed spatiotemporal expression of *rho* suggested that in addition to modulation of the Spo0A phosphorelay activity at the onset of sporulation (15), Rho might be involved in subsequent steps of spore development. To address this hypothesis, we used a set of five strains differentially expressing Rho during sporulation, namely: the WT, the strain blocked for read-through transcription of *rho* (3TER), their derivatives inactivated for *rho* expression in the forespore by the *mF-35T/A* mutation in $^{SigF}P_{rho}$ (WT-mT/A and 3TER-mT/A), and the *rho* deletion mutant (Δ*rho*).

Initially, we compared the sporulation capacities of the five strains by evaluating the asymmetric division of cells by microscopy and by counting the heat-resistant spores at the initial and final stages of sporulation, respectively. The Δ*rho* strain showed a highest proportion of cells with asymmetric septum (Fig. S3*A*) corroborating our previous data on its accelerated sporulation most probably due to efficient activation of Spo0A (15). Interestingly, asymmetric cell division was

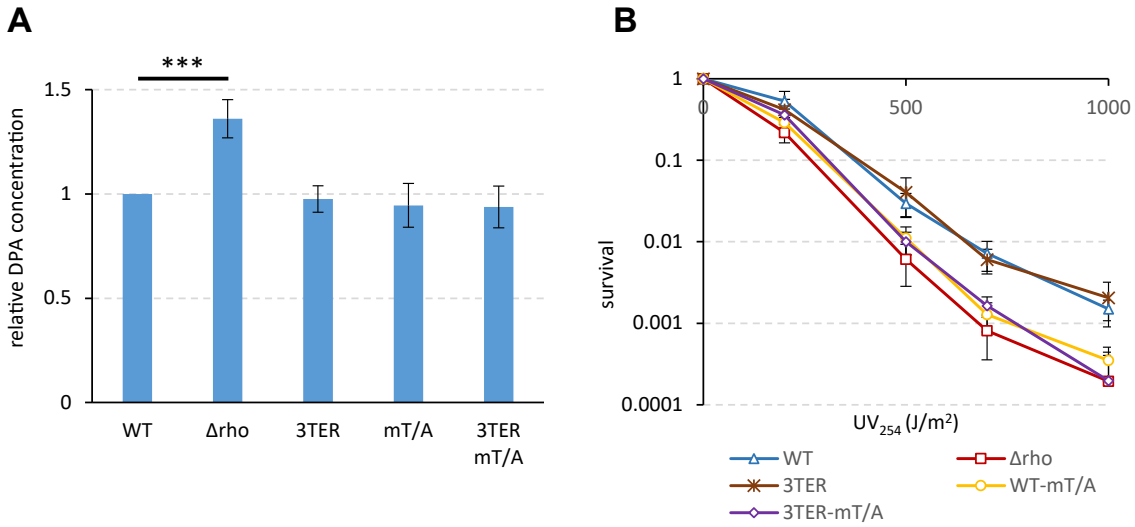

Figure 5. The alteration of the spatiotemporal expression of *rho* affects the resistance properties of mature spores. Spores produced by WT and 3TER cells expressing *rho* from the nonmodified promoters, their mutant derivatives WT-mT/A and 3TER-mT/A inactivated for *rho* expression in the forespore, and Δ*rho* cells expressing no Rho were analyzed for the levels of dipicolinic acid (*A*) and the resistance to ultraviolet irradiation (*B*) as described in Experimental procedures. *A*, spore DPA contents are normalized to the WT level. The assay was reproduced 10 times with two independently prepared sets of five spores. Plotted are mean values from all measurements. Statistical significance was estimated with a two-tailed *t* test. The displayed *p*-value is as follows: ***$p \leq 0.001$. *B*, UV test was reproduced five times with one set of spores. The bars represent SD from the mean values.

also higher in 3TER and 3TER-mT/A strains compared to WT or the WT-mT/A mutant (Fig. S3*A*), suggesting a regulatory crosstalk between Spo0A ∼ P activating read-through transcription of *rho* and Rho modulating the activity of the Spo0A phosphorelay. However, while Δ*rho* formed the heat-resistant spores at the highest rate (Fig. S3*B*) and yield (Fig. S3*C*), other mutants resembled more WT cells. Therefore, only the complete inactivation of Rho significantly affected the sporulation dynamics.

Next, we let cells sporulate for 24 h, during which more than 80 percent of cells in each strain formed spores. We then purified the spores from the five strains and compared some of their damage resistance properties. It should be noted, however, that most resistance phenotypes of spores are determined by multifactorial mechanisms, which makes their dissection difficult (reviewed in (31, 63)). All spores differentially expressing *rho* were similarly resistant to lysozyme, which targets the cortex peptidoglycan (reviewed in (64)), and became similarly sensitive to it after chemical removal of the spore coat (Fig. S4, *A* and *B*). This indicates that the permeability of the coat to lysozyme was not detectably affected by altered expression of *rho*. Likewise, all spores showed similar levels of wet-heat resistance, a complex spore phenotype determined by factors expressed in both spore compartments (Fig. S4*C*). However, Δ*rho* spores appeared to contain higher (∼35%) levels of dipicolinic acid (DPA), an important contributor to heat-resistance (reviewed in (65, 66)), than other spores (Fig. 5*A*). Interestingly, spores formed in the absence of the forespore-specific expression of *rho* (Δ*rho*, WT-mT/A and 3TER-mT/A) appeared more sensitive to ultraviolet (UV) light than WT and 3TER spores (Fig. 5*B*). This effect was spore-specific, as vegetative Δ*rho* and WT cells were equally resistant to UV radiation (Fig. S5).

Finally, we used transmission electron microscopy to analyze the ultra-structure of spores, which revealed significant differences between spores in the coat structure (Fig. 6). In accordance with numerous studies (reviewed in (64, 67, 68)), WT spores exhibited a regular coat composed of a lamellar inner layer and a striated thick electron-dense outer layer tightly attached to each other in the vast majority (over 92 percent) of spores or occasionally separated across a limited area (Fig. 6). In contrast, Δ*rho* spores contained the WT-like inner coat, but their outer coat remarkably lost electron-dense striated pattern and appeared about 50% thinner compared to WT spores (respectively, 36.2 ± 0.0091 nm and 74.2 ± 0.021 nm, as measured for 100 spores of each strain). Moreover, above 80 percent of Δ*rho* spores showed an extensive detachment of inner and outer coats, often along the entire spore perimeter (Fig. 6). Spores differentially expressing *rho* showed intermediate ranges of coat modifications. The outer coat of 3TER spores appeared less striated and electron-dense compared to WT, therefore resembling that of Δ*rho*, but remained attached to the inner layer in all analyzed spores (Fig. 6). WT-mT/A spores contained the electron-dense and striated outer coat similar to WT, but ∼30 percent of them exhibited the detachment of the two layers, although less extensive than in Δ*rho* spores (Fig. 6). Finally, 3TER-mT/A spores contained a low-structured outer coat locally separated from the inner coat in ∼30 percent of spores (Fig. 6). By combining these features, 3TER-mT/A spores appear most similar to Δ*rho* spores, which seems in line with the absence of sporulation-specific *rho* expression in both mutant strains.

Rho mediates spore germination and outgrowth

The ability to resume vegetative growth in favorable nutrient conditions, referred to as spore revival, is a basic spore

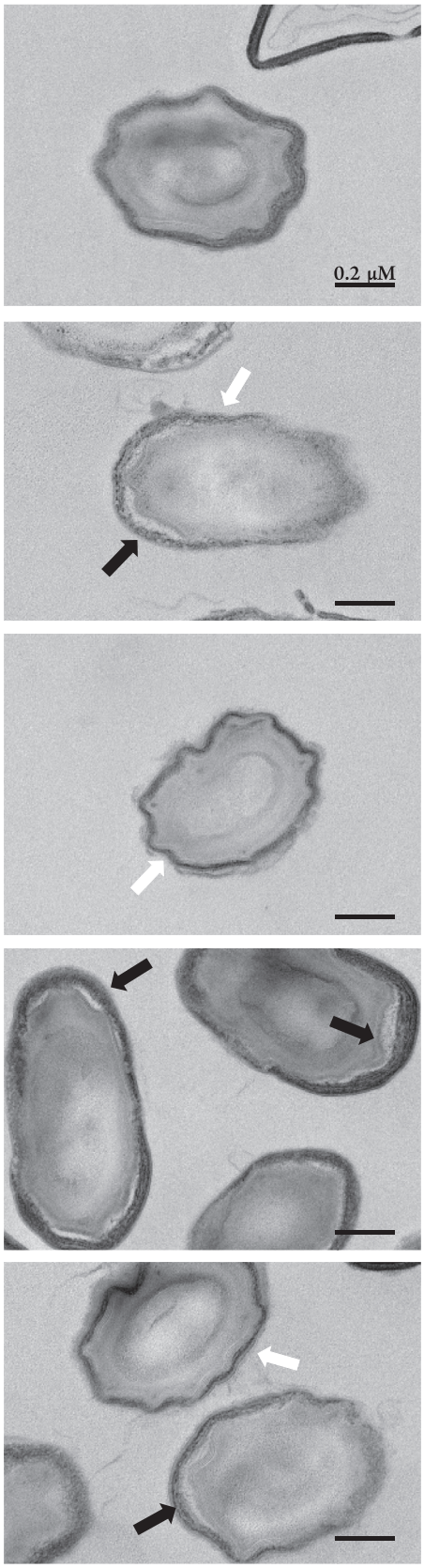

Figure 6. The alteration of the spatiotemporal expression of *rho* affects the morphology of spores. Thin section transmission electron micrographs of spores produced by cells differentially expressing *rho*. *White* arrows indicate a thinner and less electron-dense outer coat in Δ*rho*, 3TER, and 3TER-mT/A spores, which did not express *rho* in the forespores during maturation. *Black* arrows indicate the detachment of outer and inner coats in Δ*rho*, WT-mT/A, and 3TER-mT/A spores, which did not express *rho* in the mother cells.

property and spore quality indicator (64, 69–72). We compared the revival abilities of spores differentially expressing *rho* by evaluating the optical density (A_{600}) of spore suspensions after the induction of germination. Rapid rehydration and structural changes of the germinating spores alter their optical properties resulting in a decrease in A_{600}. The A_{600} of reviving spores remains stable during the post-germination phase of metabolic resumption and molecular reorganization, designated the "ripening period", before increasing later during spore outgrowth, when the emerging cells start to grow and divide (32, 73). For simplicity, we consider the outgrowth period as a time needed for a spore culture to restore its initial A_{600} after germination.

We induced spore germination with the germinants L-alanine, AGFK (a mixture of L-asparagine, glucose, fructose and potassium chloride) and L-valine recognized by different spore germinant receptors. In response to any germinator, Δ*rho* spores lost A_{600} faster than other spores, therefore showing the highest germination rate (Figs. 7*A* and S6). In contrast, the outgrowth of Δ*rho* spores in a defined minimal medium was significantly delayed compared to other spores (Fig. 7*B*), although their viability during germination was not affected (Fig. S7). The enrichment of the growth medium by casamino acids (0.5%) increased the outgrowth rate of Δ*rho* spores, which nevertheless remained below the WT level (Fig. S7*C*).

We asked whether appropriate spore revival requires the expression of *rho* during spore morphogenesis or, in addition, during outgrowth. To this end, we replaced both promoters of the *rho* gene by the IPTG-inducible promoter P_{spac}, which allowed us to selectively control *rho* expression during sporulation and/or spore outgrowth. We assumed that if the normal outgrowth of spores depends on simultaneous expression of the *rho* gene, then spores formed in the absence of Rho protein, but expressing *rho* after germination, will exhibit an outgrowth rate characteristic to WT spores. On the other hand, if only spores expressing *rho* during morphogenesis can properly resume growth, their outgrowth rate will be equivalent to WT regardless of whether *rho* was expressed after germination or not. By immunoblot analysis of cells carrying the P_{spac}-*rho* transcriptional fusion, using a Rho^{Bs}-specific antiserum, we established that the induction of P_{spac} by 100μM IPTG determines a near-natural level of Rho protein. Next, we produced the mature P_{spac}-*rho* spores in the absence or presence of 100μM IPTG and compared their revival under conditions when IPTG was added to the growth medium to induce *de novo* expression of *rho* or was omitted. In both conditions, spores that were formed in the absence of IPTG and therefore did not express *rho* during morphogenesis (P_{spac}-*rho* $^{(+IPTG)}$ spores) germinated as fast as Δ*rho*. In contrast, spores that were expressing *rho* during their formation due to IPTG (P_{spac}-*rho* $^{(+IPTG)}$ spores) germinated like WT

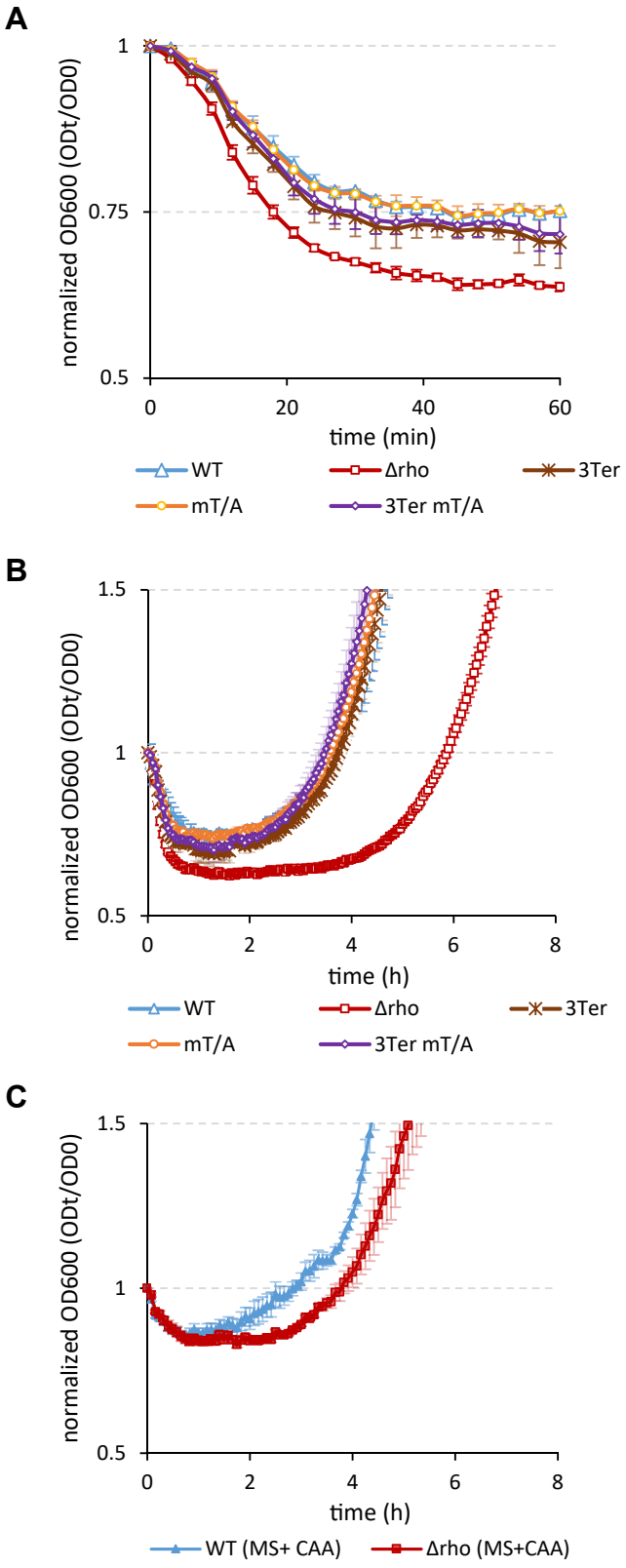

Figure 7. Rho activity determines the revival properties of spores. Spores of the WT (*blue triangles*), Δ*rho* (*red squares*), 3TER (*brown* crosses), WT-mT/A (*orange circles*), and 3TER-mT/A (*violet diamonds*) strains were induced by the germinant L-alanine (10mM) and compared for germination (*A*) and outgrowth in the nutrient-poor MS medium (*B*) as described in Experimental procedures. *C*, WT (filled-in *blue triangles*) and Δ*rho* (filled-in *red squares*) spores were germinated as in (*A*) and analyzed for outgrowth in the nutrient-replenished MS medium containing 0.5% casamino acids. The experiments were performed at least twice with three independent sets of spores. Each experiment included up to six replicas of individual suspensions of spores. The results of the representative experiment are plotted. The bars represent SD from the mean values.

spores (Figs. 8*A*, S9). When IPTG was omitted from the medium, the outgrowth of the germinated P_{spac}-*rho* $^{(-IPTG)}$ spores was similar to Δ*rho*, while the outgrowth rate of P_{spac}-*rho*$^{(+IPTG)}$ spores was significantly higher, although remained below the level of WT spores (Fig. 8*B*). The outgrowth of both types of spores slightly accelerated when IPTG was added to the medium, most probably due to the induction of *rho* (Fig. 8*C*). This small stimulatory effect of IPTG was however sufficient for P_{spac}-*rho*$^{(+IPTG)}$ spores to reach the outgrowth rate characteristic of WT spores, while the outgrowth of P_{spac}-*rho* $^{(-IPTG)}$ spores spores remained close to the Δ*rho* level (Fig. 8*C*).

We concluded that efficient revival of spores mainly requires the expression of *rho* during spore morphogenesis, but also, although to a lesser extent, during spore outgrowth.

Discussion

The main achievement of the present study is the revelation of spatiotemporal expression of the termination factor Rho during *B. subtilis* sporulation *via* two distinct mechanisms: read-through transcription initiated at a distal SigH-controlled promoter in the mother cells, and transcription from an authentic SigF-dependent *rho* promoter in the forespores. These regulatory elements compensate for the decrease of *rho* expression due to the silencing of the vegetative SigA-dependent *rho* promoter and allow the "refueling" of Rho protein in both compartments of the sporangium. Such a specific pattern of *rho* expression is important for the formation of spores with normal morphology, resistance properties and the ability to return to a vegetative state.

The sporulation-specific transcription of *rho* is initiated by the activation of the SigH-dependent promoter of *spo0F* gene, encoding the phosphotransferase Spo0F of the Spo0A phosphorelay. The expression of *spo0F* is regulated by Spo0A ~ P and constitutes one of the positive feedback loops of Spo0A ~ P at the onset of sporulation (53–56, 74). At the same time, modulation of Spo0A ~ P activity at the initial steps of *B. subtilis* differentiation requires a decrease in *rho* expression levels (15). It appears that alongside a self-reinforcing loop involving Spo0F, Spo0A ~ P simultaneously activates the Rho-mediated regulatory circuit, which can be viewed as a negative feedback loop of Spo0A ~ P. This regulatory function of Rho could be particularly important to fine-tune Spo0A ~ P activity in mother cells, where Spo0A ~ P remains functional after asymmetric division (75). Moreover, inhibition of the read-through transcription of *rho* results in the structural changes of spore coat, whose assembly depends on the activity of SigE- and SigK-controlled genes (41, 64, 68). This emphasizes the importance of Rho activity during the mother cell gene expression program.

Identification of the alternative forespore-specific *rho* promoter matching the SigF-binding consensus allows us to

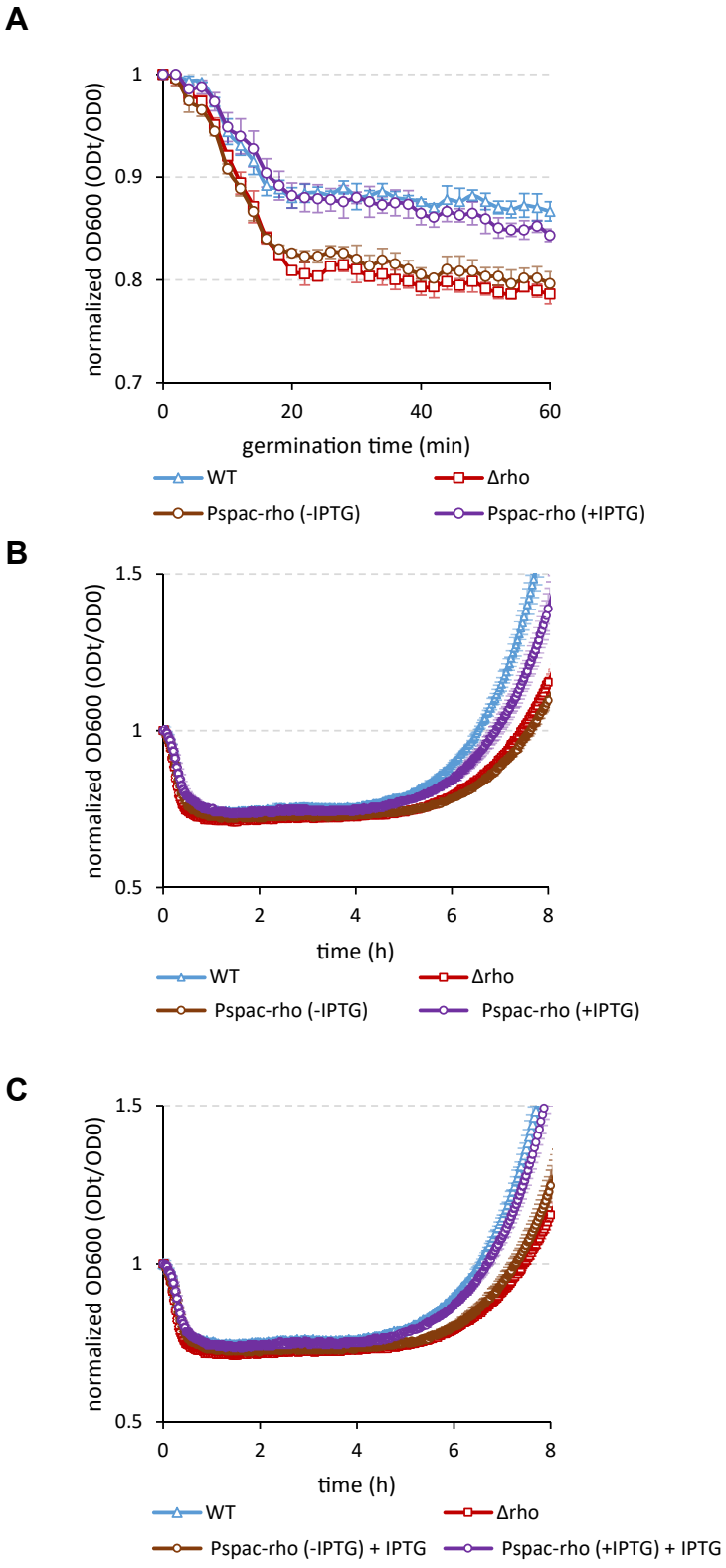

Figure 8. The WT rate of spore outgrowth requires the expression of *rho* during spore morphogenesis and *de novo* after germination. Spores of the WT P_{spac}-*rho* strain expressing Rho protein from the IPTG-inducible promoter P_{spac} were produced in the absence (*brown circles*) or presence (*violet circles*) of IPTG 100μM and compared with the WT (*blue triangles*) and Δ*rho* (*red squares*) spores for germination with L-alanine (*A*) and outgrowth in MS medium without (*B*) or with IPTG 100mM (*C*). Of note, induction of rho expression by IPTG (*C*) slightly accelerates the outgrowth compared to (*B*). The experiments were reproduced at least twice with two independent samples of the IPTG-induced or noninduced WT P_{spac}-*rho* spores. Each experiment included up to six replicas of individual suspensions of spores. The results of the representative experiment are plotted. The bars represent SD from the mean values.

classify *rho* as a member of the SigF regulon. Although an earlier analysis of forespore gene expression detected an up-regulation of *rho* in sporulating *sigF* $^{+}$ *B. subtilis* cells, *rho* was not induced by the artificial expression of SigF during exponential growth (44). It is possible that, in that study, the untimely expressed SigF failed to compete with the abundant vegetative SigA for binding to the overlapping cognate *rho* promoters. The silencing of the SigA-dependent *rho* promoter might facilitate SigF binding. It is also notable that the *rho* gene is located within a chromosomal cluster of SigF-dependent genes entering the prespore at the time of SigF activation (43, 44). Early activation of *rho* may be important for the proper expression of the late forespore-specific genes, such as SigG-regulated genes that determine the resistance of spores to ultraviolet radiation (76–78). It may also undelay the presence of Rho in mature spores, as recently shown by mass spectrometry (79, 80).

Our previous transcriptome analyses of Δ*rho* cells during the exponential growth and in stationary phase revealed disordered and untimely expression of many sporulation genes *via* their extensive sense or antisense read-through transcription and unscheduled activation of promoters (Table S1; the expression profiles can be visualized at http://genoscapist.migale.inrae.fr/seb_rho/ (16, 81)). We are aware that most of the potential sporulation-specific targets of Rho are not yet expressed in the conditions used for RNAseq analyses. However, we suggest that at least some of sporulation genes abnormally expressed in the stationary Δ*rho* cells are subject to Rho-mediated regulation during sporulation. Some of them are worth discussing here as potential clues for future studies.

For instance, the coat defects in Δ*rho* and 3TER-mT/A spores resemble those induced by the mutations of genes encoding the morphogenetic proteins CotO, CotH or CotG, or auxiliary proteins of coat assembly, superoxide dismutase SodA and holin YwcE, which all result in a disordered, low electron-dense and thinner outer coat frequently detached from the inner layer (64, 82–87). Among the above-mentioned genes, *cotG* is strongly up-regulated in Δ*rho* cells due to the transcription upshift at, or close to, its SigK-dependent promoter and the sense read-through transcription initiated upstream (11, 16). The same read-through transcript is antisense to the oppositely oriented neighboring *cotH* gene. It is tempting to speculate that the changes in *cotH-cotG* transcription alter the protein balance between the protein kinase CotH and its target protein CotG, which is important for proper assembly of spore coat (84, 85, 88, 89), therefore leading to structural modifications of the coat in Δ*rho* spores. Other potential targets of Rho-mediated regulation may certainly exist among at least 80 proteins involved in the spore coat formation (67, 68).

Besides the phenotypes linked to the inhibition of spatiotemporal expression of *rho*, the Δ*rho* spores are specifically altered in revival capacity characterized by rapid germination and slow outgrowth. The rate of germination in response to different nutrient stimuli is mainly determined by the levels of corresponding germinant receptors in the spore membrane (90–92). In line with this, the Δ*rho* transcriptomes attest for the increased expression of the *gerBA-gerBB-gerBC* operon encoding the AGFK germinant receptor GerB (93) and the *gerPA-gerPB-gerPC-gerPD-gerPE-gerPF* operon, whose products facilitate the passage of nutrient germinants across the spore coat (94). Among the *gerAA-gerAB-gerAC* genes encoding the L-alanine germinant receptor GerA [(94, 95), and references therein], only *gerAA* is up-regulated in the stationary Δ*rho* cells. However, it is notable that *rho* was identified among the genes whose inactivation by Mariner transposon results in a premature GerA-mediated germination of the developing spores (46, 71). The germination of **Δ***rho* spores might be also influenced by high levels of DPA, a potent non-nutrient germinant that is also involved in the nutrient-induced germination (96, 97). More generally, a synchronous and rapid sporulation of **Δ***rho* cells might result in a population of structurally homogeneous spores and, consequently, in a decreased heterogeneity of spore germination (15, 34, 35, 98–100).

Unlike germination, the outgrowth of the germinated *Δrho* spores is slowed even in a nutrient-enriched medium. Therefore, *rho* inactivation imposes more stringent requirements for spore outgrowth, which in itself is more exacting than vegetative growth (101). We show that normal outgrowth of spores requires *rho* expression both during sporulation and after germination. During sporulation, Rho would ensure a proper composition of a spore "molecular cargo" required for revival, which also includes Rho protein itself (34, 79, 100). After germination, Rho would act in the ripening period, and later, during implementation of the transcription program of vegetative growth. This is consistent with the differential gene expression analysis of the reviving *B. subtilis* spores, which detected the upshifts in *rho* expression shortly after germination and at the end of outgrowth (79). Most probably, the resumption of *rho* expression during outgrowth reflects the reactivation of the SigA-dependent *rho* promoter. Taken together, a rapid germination and a slow outgrowth of Δ*rho* spores suggest that Rho influences the spore-revival fitness.

To conclude, this and our previous analyses trace the activity of Rho through each stage of the complex program of *B. subtilis* sporulation, from the regulation of Spo0A ∼ P activation at the onset of sporulation, through the subsequent morphogenesis of spores and up to the modulation of spore revival. This suggests the existence of specific targets for Rho-mediated transcription termination within the regulon of each alternative Sigma factor, which certainly include, alongside the known coding genes, a set of non-coding and antisense transcripts. Appropriate regulation of these targets requires in turn an accurate time- and spatial-specific regulation of the *rho* expression, through the mechanisms we describe.

Experimental procedures

Bacterial strains and growth conditions

All strains used in the analysis originate from *B. subtilis* 168 *trp* $^{+}$ strain BSB1 (11) and are listed in Table S2. The *E. coli* TG1 strain was used for construction of intermediate plasmids. Cells were routinely grown in liquid or solidified

lysogeny broth (LB) medium at 37 °C. Standard protocols were used for transformation of *E. coli* and *B. subtilis* competent cells (102). Sporulation of *B. subtilis* cells was induced by the method of nutrient exhaustion in supplemented DSM (Difco) (103) or by the resuspension method (102), as detailed in (16). Optical density of the bacterial cultures was measured with NovaspecII Visible Spectrophotometer, Pharmacia Biotech. When required, antibiotics were added at following concentrations: 0.5 μg per ml of erythromycin, 3 μg per ml of phleomycin, 100 μg per ml of spectinomycin, and 5 μg per ml of chloramphenicol to *B. subtilis* cells; and 100 μg per ml of ampicillin or 20 μg per ml of kanamycin to the plasmid-containing *E. coli* cells. For the induction of P_{spac}-*rho* fusion, IPTG inducer was added to cells and spores to final concentration 100μM.

Strains and plasmids construction

All intermediate plasmids were constructed using Q5 High Fidelity DNA Polymerase and DNA modification enzymes purchased from New England Biolabs. Transcriptional fusion of the luciferase gene *luc* and the *rho* promoter (P_{rho}-*luc*) was constructed as follows. The oligonucleotide pairs glpXBam/veb738 were used to amplify a ∼1 Kb fragment of *B. subtilis* chromosome located directly upstream the *rho* start codon. The 5′ part of the *luc* gene was amplified from the plasmid pUC18cm-Luc (52) using oligonucleotides *lucintrev* and veb739 complementary to veb738. Two DNA fragments were joined by PCR using the primers glpXBam and *lucintrev*, and the resulting DNA fragment was cloned at pUC18cm-Luc using BamHI and BstBI endonucleases and T4 DNA ligase. The resulting plasmid pBRL862 was integrated by single crossover at the *rho* chromosomal locus of BSB1 (WT) and BRL1 (Δ*rho*) cells using selection for chloramphenicol-resistance. By this event, the *luc* gene was placed under all natural regulatory signals of the *rho* expression. In the WT background, the replaced intact copy of *rho* gene remained active under the control of own promoter.

Insertion of three intrinsic transcription terminators (3TER) upstream the chromosomal P_{rho}-*luc* fusion was performed as follows. The 3TER DNA fragment amplified from pMutin4 plasmid using oligonucleotides veb734 and veb735 was end-joined with the DNA fragments amplified from pBRL862 using the pairs of oligonucleotides glpXBam/veb798 (5′-complementary to veb734) and *lucintrev*/veb797 (5′-complementary to veb735). The primers glpXBam and *lucintrev* were used in the joining reaction. The PCR product was cut by EcoRV and BstBI endonucleases and cloned at a similarly cut and gel-purified pBRL862 plasmid. The resulting plasmid pBRL1107 was integrated at the *rho* locus of BSB1 chromosome as above. The created 3TER-P_{rho}-*luc* transcriptional fusion contains intact 5′-UTR of *rho* and the 3TER insertion immediately after the *glpX* stop codon.

Transcriptional fusion between the *gfp* gene, encoding Green Fluorescent Protein, and the *rho* promoter (P_{rho}-*gfp*) was constructed similarly to P_{rho}-*luc*. The oligonucleotides glpXBam and veb742 were used for amplification of the *rho* moiety from BSB1 chromosome, and the *gfp* gene was amplified from the plasmid pCVO119 using the primers veb741 and veb740 complementary to veb742. The primers glpXBam and veb741 were used for joining PCR, and the resulting DNA fragment was cloned in pCVO119 plasmid using BamHI and NcoI endonucleases and T4 DNA ligase. The resulting plasmid pBRL893 was integrated by single crossover at the *rho* locus of the BSB1 chromosome using selection for spectinomycin resistance.

To construct the 3TER-P_{rho}-*gfp* transcriptional fusion, the DNA fragment containing 3TER and the *rho* 5′-UTR was amplified from pBRL1107 plasmid using the primers glpXBam and veb742 and fused to the *gfp* gene as described above for pBRL893. The product of joining PCR was cut by EcoRV and NcoI endonucleases and cloned at a similarly cut and gel-purified pBRL893. The resulting pBRL1150 plasmid was inserted in the BSB1 chromosome as above.

Site-directed mutagenesis of the Sigma F-dependent *rho* promoter of the P_{rho}-*luc* and P_{rho}-*gfp* transcriptional fusions was performed as follows. The plasmids pBRL893 and pBRL1107 were entirely amplified using the pairs of side-by-side oligonucleotides veb803/veb802, containing a 5′-terminal C nucleotide to introduce the point mutation *mF-35T/C*, and veb803/veb805, with a 5′-terminal A for the point mutation *mF-35T/A*. The PCR products were phosphorylated using T4 polynucleotide kinase, self-ligated and treated with DpnI endonuclease to remove the template DNA prior transformation in *E. coli* cells. The resulting mutated derivatives of the plasmids pBRL893 (pBRL1141 and pBRL1164) and pBRL1107 (pBRL1116 and pBRL1162) were controlled by sequencing and inserted into the *B. subtilis* BSB1 chromosome as above to produce the mutated fusions *mF-35T/C* P_{rho}-*gfp* and *mF-35T/A* P_{rho}-*gfp* and 3TER *mF-35T/C* P_{rho}-*luc* and 3TER *mF-35T/A* P_{rho}-*luc*, respectively.

All strains constructed by single crossover recombination were tested for the absence of potential insertion of the plasmid oligomers. This was performed by PCR using oppositely oriented primers veb960 and veb961, which would provide amplification of plasmid DNA only if tandem copies of it were present in the chromosome. The absence of such specific amplification indicates that cells contain a single copy of the reporter fusion, and only such strains were used in the analysis.

Structural modifications of the *rho* expression unit at natural locus were performed by the method for allelic replacement using a shuttle vector pMAD (104).

To insert 3TER transcription terminators at the *rho* locus, two DNA fragments amplified from the BSB1 chromosome with the pairs of oligonucleotides veb795/veb796 and veb797/veb798 were end-joined to the 3TER DNA fragment (see above) by PCR using the primers veb795 and veb796. The product of joining PCR was cut with BamHI and EcoRI endonucleases and cloned in the pMAD vector (104). The resulting plasmid pBRL1108 was integrated into the *rho* locus of the BSB1 chromosome with selection of the erythromycin-resistant transformants at 37 °C non-permissive for plasmid replication. Single transformants were propagated in LB without antibiotic at 30 °C to induce the loss of the vector and

platted at LB-plates at 37 °C. The erythromycin-sensitive clones were selected among the grown colonies and tested by PCR for the presence of the 3TER insertion using oligonucleotides veb734 and veb735, and the selected clones were controlled for structural integrity of the *glpX-3TER-rho* region by sequencing.

The point mutation *mF-35T/A* was introduced in the *rho* locus of BSB1 and BRL1130 (3TER) strains as follows. Two DNA fragments were amplified from pBRL1164 plasmid and BSB1 chromosome by PCR with the respective pairs of oligonucleotides veb796/veb808 and veb806/veb807, complementary to veb808. The fragments were joined by PCR using veb796 and veb806 as primers, and the resulting product was cloned at pMAD vector using BamHI and EcoRI endonucleases and T4 DNA ligase. The resulting plasmid was transformed into BSB1 cells and the transformants were processed as described above to select the point mutant WT-mT/A. The mutant strain 3TER-mT/A was constructed in a similar way using the plasmid pBRL1162 as a template in the first PCR and WT-mT/A strain as a recipient for transformation.

To construct the IPTG-controlled system for *rho* expression, the DNA fragment amplified from BSB1 chromosome by PCR with the oligonucleotides veb806 and veb880 was digested by EcoRI and BamHI endonucleases and clones at pMUTIN4 vector (57). The resulting plasmid was transformed in BSB1 cells with selection to erythromycin resistance.

For the purification of the *B. subtilis* Rho protein, *rho* gene was amplified by PCR with oligonucleotides veb596 and veb599, treated by NdeI and SalI endonucleases and cloned at the expression vector pET28a (Novagen) allowing expression of Rho with N-terminal hexa-histidine tag. The resulting plasmid pETRho was transferred to *E. coli* strain BL21-CodonPlus (DE3)-RIL (Stratagene).

Luciferase assay

Analysis of promoters' activity using luciferase fusions was performed as described previously (52) with minor modifications detailed in (16). Cells were grown in LB medium to mid-exponential phase (A_{600} 0.4–0.5), cultures were centrifuged and resuspended to A 1.0 in fresh LB or DSM, to follow expression of the fusions during growth or sporulation, respectively. The pre-cultures were next diluted in respective media to A_{600} 0.025. The starter cultures were distributed by 200µl in a 96-well black plate (Corning) and Xenolight D-luciferin K-salt (Perkin) was added to each well to a final concentration of 1.5 mg/ml. The cultures were grown under strong agitation at 37 °C and analyzed in Synergy 2 Multi-mode microplate reader (BioTek Instruments). Relative luminescence units and A_{600} were measured at 5 min intervals. Each fusion-containing strain was analyzed at least three times. Each experiment included four independent cultures of each strain.

Epifluorescence microscopy and image processing

For all microscopic observations, cells were mounted on a 2% agarose pad and topped with a coverslip. Bacteria were imaged with an inverted microscope (Nikon Ti-E) equipped with an iLas2 laser coupling system from Roper Scientific (150 mW, 488nm and 50 mW, 561 nm), a 100 × oil immersion phase objective, an ORCA-R2 camera (Hamamatsu) and controlled by the MetaMorph software package (v 7.8; Molecular Devices, LLC). The post-acquisition treatment of the images was done with the Fiji software (105, 106). To determine the frequency of cells entering into sporulation, cultures were sampled 3 hours after the induction of sporulation by the resuspension method (102). Sampled cells were mixed with the lipophilic fluorescent dye Mitotracker Red (10 µg/ml final concentration) prior to microscopic observation. Asymmetric septa were manually counted in three independent replicas ($N > 500$ per strain and per replica).

To assess *rho* expression during sporulation using GFP as a reporter, cells bearing the non-modified or the point-mutated P_{rho}-*gfp* transcriptional fusions were induced for sporulation by the resuspension method and sampled as above. Sampled cells were mixed with the lipophilic fluorescent dyes Nile Red (10 µg/ml final concentration) prior to microscopic observation. To measure the fluorescence intensity in the different compartments, circular areas of a constant 0.45 µm diameter were drawn in the center of individual compartments (forespores, mother cells, or predivisional cells) using images showing membrane-labelled cells, and recorded as a list of ROI. ROIs were subsequently applied over the corresponding image displaying the GFP signal, and the average fluorescence over each ROI recorded. Background fluorescence, determined as the average fluorescence from ROIs of identical areas spread over the field (outside cells), was subtracted to give the final fluorescence intensity of individual compartments. Counting was performed in at least two fields of view and for a minimum of 100 cell compartments per strain, per replica. Plotted values are average fluorescence intensities from a representative experiment. Statistical significance was determined by *t* test.

RNA preparation and Northern blotting

Total RNA was extracted from the 10-ml *B. subtilis* cultures at A_{600} indicated in the text by the glass beads method (107). For Northern blotting, 5 µg of RNA were separated on 1% agarose-formaldehyde (2.2M) gel in MOPS (50mM)/EDTA (1mM) buffer (pH 7.0) and transferred to Hybond N+ membrane (GE-Healthcare) as described previously (108). Membrane pre-hybridization and the *rho* RNA detection by hybridization with the *rho*-specific α^{32}P -labelled riboprobe was performed as detailed in (109). The riboprobe was synthesized by T7 RNA polymerase in the presence of [α-^{32}P]UTP at the template of the purified PCR fragment obtained with oligonucleotides YRH1 and YRH2 (Table S3). The reverse PCR primer YRH1 contained at the 5′-end the T7 RNA polymerase promoter sequence (TAATACGACTCACTATA).

Sporulation assay

Cells were induced for sporulation by the resuspension method, and the cultures were analyzed for the presence of spores starting from 6 hours after resuspension. The percentage of spores in a sample was calculated as proportion of

viable cells after heating at 70 °C for 15 min to the total number of cells as described in (16).

Spore purification and treatments

B. subtilis cells growing exponentially in LB were suspended in DSM at A_{600} 0.05 and cultured at 37 °C with aeration for 24 h. Spores were purified by sequential rounds of intensive washing in ice-cold water and centrifugation over 3 days as described in (103). The samples of the purified spores were controlled for the absence of cells by the heat-resistance test as described above and stored at 4 °C in water at $A_{600} > 10$. The purity of standard spore samples was above 95 percent.

For electron microscopy analysis, spores were additionally purified on Nicodenz (Axis-Shield) density gradients. Spores were suspended in 1 ml of 20% Nicodenz solution, layered on 50% Nicodenz (15 ml) in the centrifuge tubes and centrifuged at 14,000*g* for 30 min at 10 °C. The pelleted pure spores were washed 5 times in ice-cold water to remove traces of Nicodenz and kept at 4 °C before analysis.

Prior the assays of spore resistance phenotypes and germination, the purified spores were suspended in 10 mM Tris HCl (pH 8.0) at A_{600} 1.0 and activated by heating at 70 °C for 30 min and subsequent cooling in ice for 20 min. The activated spores were used in the assays within 1 h.

Chemical removal of spore coats was performed according to (110). Spores were suspended in decoating solution (50 mM Tris base, 8 M urea, 50 mM dithiothreitol, 1% sodium dodecyl sulfate; pH 10.0) at A_{600} 5.0 and incubated at 60 °C for 90 min with vortexing. After the treatment, spores were intensively washed in STE buffer (150 mM NaCl, 10 mM Tris-HCl, 1 mM EDTA; pH 8.0) as described.

Transmission electron microscopy

Purified spores were fixed with 2% glutaraldehyde in 0.1 M sodium cacodylate buffer (pH 7.2) for 1 h at room temperature. Samples were contrasted with 0.5% Oolong tea extract in cacodylate buffer and postfixed with 1% osmium tetroxide containing 1.5% potassium cyanoferrate. The samples were dehydrated and embedded in Epon (Delta Microscopies), as described (111). Thin sections (70 nm) were collected onto 200-mesh copper grids and counterstained with lead citrate. Grids were examined with a Hitachi HT7700 electron microscope operated at 80 kV, and images were acquired with a charge-coupled device camera (Advanced Microcopy Techniques; facilities were located on the MIMA2 platform [INRAE; https://doi.org/10.15454/1.5572348210007727E12]). The post-acquisition treatment of the images and measurement of the thickness of the spore coat were performed using the Fiji software (106).

Spore UV resistance assay

The activated spores were suspended in Tris-HCl (pH 8.0) at A_{600} 0.5, pipetted in triplicates (50µl) in the wells of 48-well sterile microtiter plates (Evergreen Scientific) and irradiated by ultraviolet (254 nm) light using Stratalinker 2400 UV Crosslinker (Stratagene) at the J/m^2 doses indicated in the text (one plate per UV dose). The irradiated spore suspensions were plated in sequential dilutions at LB plates and the colonies were counted after 24 h of incubation at 37 °C. The UV-resistance was determined as a ratio of the colony-forming units in the irradiated and non-irradiated samples of spores. Five experiments were performed with two independent sets of spores differentially expressing Rho.

To determine the effect of *rho* inactivation on the UV resistance of vegetative cells, WT and Δ*rho* cultures in the late exponential phase (~10^8 cells/ml) were plated on LB plates and irradiated with the increasing doses of UV (254 nm) light using a Stratalinker 2400 UV Crosslinker (Stratagene). The UV-resistance of cells was estimated as above. Three independent experiments were performed.

DPA assay

The DPA content of spores was analyzed according to the protocol of Nicholson and Setlow in (102).

Spore germination and outgrowth assay

Spore germination and outgrowth assays were performed in MS medium (10.8 g l^{-1} of K_2HPO_4, 6 g l^{-1} of KH_2PO_4, 1 g l^{-1} of $C_6H_5Na_3O_7.2H_2O$, 0.2 g l^{-1} of $MgSO_4.7H2O$, and 2 g l^{-1} of K_2SO_4) supplemented with 0.5% glucose, 0.01% L-tryptophan, 0.1% glutamate, 0.1 mM of $FeCl_3$ citrate, 0.1 mM of $CaCl_2$, 1 mM of $MgSO_4$ and trace elements (0.001 g l^{-1} of $MnCl_2$ $4H_2O$, 0.0017 g l^{-1} of $ZnCl_2$, 0.00043 g l^{-1} of $CuCl_2{\cdot}2H_2O$, 0.0006 g l^{-1} of $CoCl_2$ $6H_2O$ and 0.0006 g l^{-1} of $Na_2MoO_4{\cdot}2H_2O$). The stock solutions (100mM) of L-alanine and L-valine germinants were prepared in 10 mM Tris-HCl buffer (pH 8.0) containing 10mM D-glucose and 100mM KCl. The stock solution of AGFK germinant mixture contained 100 mM L-asparagine, 10mM D-glucose, 10 mM D-fructose and 100mM KCl in 10 mM Tris-HCl buffer (pH 8.0). The activated spores were diluted to A_{600} 0.2 in the cold MS medium and distributed by 135 µl in the 96-well plate. Spore suspensions were simultaneously induced for germination by adding 15µl of a stock germinant solution, incubated under strong agitation at 37 °C and monitored for A_{600} at 2 min intervals in Synergy 2 Multimode microplate reader (BioTek Instruments). It usually took ~1 min between germinant addition and the first A_{600} reading. When needed, the stock solution of the germinant L-alanine was supplemented with 1mM IPTG or 5% casamino acids to get their final concentrations in spore suspensions 100µM and 0.5%, respectively. Three independently prepared sets of spores were used in the analysis. The assays were performed with each set of spores at least twice and included up to six replicas of each spore suspension in the same plate.

Purification of the B. subtilis *Rho protein for antibody preparation*

E. coli BL21-CodonPlus (DE3)-RIL cells containing pETRho were grown to an A_{600} of 0.2 in a 400 ml culture (2YT medium) at 16 °C, and Rho expression was induced by the addition of 0.5 mM IPTG with continued growth overnight. The culture was harvested, pelleted and frozen at −80 °C until further use. The frozen cells were resuspended in 10 ml of lysis buffer at 4

°C containing 20 mM Tris–HCl pH 9.0, 100 mM Na_2HPO_4, 0.3 M NaCl, 10% glycerol and 0.1% Triton X-100, to which were added 10 mg/ml DNase I and an EDTA-free anti-protease tablet (Roche). The suspension was passed twice through a French press (20,000 p.s.i.) and the lysate centrifuged for 30 min at 15,000*g*. Imidazole-HCl (pH 8.0) was added to the supernatant to give a final concentration of 1 mM and the resultant suspension was applied to a 1 ml Ni^{2+}-NTA column (Qiagen). The resin was then washed sequentially with 10 ml of lysis buffer (without Triton X-100), 10 ml of buffer containing 20 mM Tris–HCl pH 9.0, 0.3 M NaCl, 20 mM Imidazole and, finally, 10 ml 20 mM Tris–HCl pH 9.0, 0.3 M NaCl and 250 mM Imidazole. *B. subtilis* Rho was eluted with 20 mM Tris–HCl pH 9.0, 100 mM Na_2HPO_4, 0.3 M NaCl and 500 mM Imidazole as 1ml fractions into collection tubes pre-filled with 3 ml elution buffer lacking Imidazole, to immediately dilute the sample 4-fold and avoid precipitation. The protein peak was determined initially by measuring the protein concentration (Bio-Rad) in the different fractions. Peak fractions were pooled and dialyzed over-night in buffer containing 20 mM Tris–HCl pH 9.0, 100 mM Na_2HPO_4, 0.3 M NaCl, 10% glycerol. Protein purity was verified by SDS–PAGE analysis and estimated at >95%. A sample of purified *B. subtilis* Rho protein at 1.1 mg/ml in storage buffer was filtered through 5µm, 0.5µm and then 0.2µm Acrodisk filters before rabbit immunization to generate custom anti-Rho polyclonal antibodies through the commercial '87-days anti-antigen classical' program of Eurogentec. The low solubility of *B. subtilis* Rho in buffers suitable for immobilization on affinity chromatography columns prevented further purification of the anti-Rho antibodies from the crude sera. The best anti-Rho serum aliquot was selected from the immunization program aliquots by Western blotting with purified *B. subtilis* Rho and *B. subtilis* cell extract samples.

Western blotting

The crude cell extracts were prepared using Vibracell 72,408 sonicator (Bioblock scientific). Bradford assay was used to determine total protein concentration in each extract. Equal amounts of total proteins were separated by SDS-PAGE (10% polyacrylamide) alongside the Color Prestained Protein Standard (New England Biolabs). After the run, proteins were transferred to Hybond PVDF membrane (GE Healthcare), and the transfer quality was evaluated by staining the membrane with Ponceau S (Sigma-Aldrich). The Rho protein was visualized by hybridization with antiserum against *B. subtilis* Rho (Eurogentec; dilution 1:5000) and the secondary peroxidase-coupled anti-rabbit IgG antibodies A0545 (Sigma-Aldrich; dilution 1:20,000).

Data availability

All data are contained within this manuscript. All described strains and plasmid constructs are available upon request from the corresponding author.

Supporting information—This article contains supporting information (11, 15, 57, 74, 104, 105, 112–116).

Acknowledgments—We are grateful to the INRAE MIGALE bioinformatics facility (doi: 10.15454/1.5572390655343293E12) for storage resources.

Author contribution—V. B. and E. B. writing–original draft; V. B., A. C., C. P., Y. R.-H., and E. B. visualization; V. B. project administration; V. B., A. C., C. P., Y. R.-H., O. P., S. D., and E. B. investigation; V. B. and E. B. conceptualization; A. C. and C. C. writing–review and editing; A. C. formal analysis; C. C., M. B., and M. J. resources; E. B. funding acquisition.

Funding and additional information—This work was supported by the grant (ANR-18-CE12-0025) from the French National Research Agency (https://anr.fr).

Conflict of interest—The authors declare that they have no conflicts of interest with the contents of this article.

Abbreviations—The abbreviations used are: DPA, dipicolinic acid; DSM, Difco Sporulation Medium.

References

1. Peters, J. M., Vangeloff, A. D., and Landick, R. (2011) Bacterial transcription terminators: the RNA 3′-end chronicles. *J. Mol. Biol.* **412**, 793–813
2. Ray-Soni, A., Bellecourt, M. J., and Landick, R. (2016) Mechanisms of bacterial transcription termination: all good things must end. *Annu. Rev. Biochem.* **85**, 319–347
3. Kriner, M. A., Sevostyanova, A., and Groisman, E. A. (2016) Learning from the leaders: gene regulation by the transcription termination factor Rho. *Trends Biochem. Sci.* **41**, 690–699
4. Turnbough, C. L., Jr. (2019) Regulation of bacterial gene expression by transcription attenuation. *Microbiol. Mol. Biol. Rev.* **83**, 10–1128
5. Mandell, Z. F., Zemba, D., and Babitzke, P. (2022) Factor-stimulated intrinsic termination: getting by with a little help from some friends. *Transcription* **13**, 96–108
6. Roberts, J. W. (1969) Termination factor for RNA synthesis. *Nature* **224**, 1168–1174
7. Quirk, P. G., Dunkley, E. A., Jr., Lee, P., and Krulwich, T. A. (1993) Identification of a putative Bacillus subtilis rho gene. *J. Bacteriol.* **175**, 647–654
8. Peters, J. M., Mooney, R. A., Kuan, P. F., Rowland, J. L., Keles, S., and Landick, R. (2009) Rho directs widespread termination of intragenic and stable RNA transcription. *Proc. Natl. Acad. Sci. U. S. A.* **106**, 15406–15411
9. Hao, Z., Svetlov, V., and Nudler, E. (2021) Rho-dependent transcription termination: a revisionist view. *Transcription* **12**, 171–181
10. Mandell, Z. F., Vishwakarma, R. K., Yakhnin, H., Murakami, K. S., Kashlev, M., and Babitzke, P. (2022) Comprehensive transcription terminator atlas for Bacillus subtilis. *Nat. Microbiol.* **7**, 1918–1931
11. Nicolas, P., Mäder, U., Dervyn, E., Rochat, T., Leduc, A., Bidnenko, E., *et al.* (2012) Condition-dependent transcriptome reveals high-level regulatory architecture in Bacillus subtilis. *Science* **335**, 1103–1106
12. Peters, J. M., Mooney, R. A., Grass, J. A., Jessen, E. D., Tran, F., and Landick, R. (2012) Rho and NusG suppress pervasive antisense transcription in Escherichia coli. *Genes Dev.* **26**, 2621–2633
13. Mäder, U., Nicolas, P., Depke, M., Pané-Farré, J., Debarbouille, M., van Dijl, J. M., *et al.* (2016) Staphylococcus aureus transcriptome architecture: from laboratory to infection-mimicking conditions. *PLoS Genet.* **1**, e1005962
14. Botella, L., Vaubourgeix, J., Livny, J., and Schnappinger, D. (2017) Depleting Mycobacterium tuberculosis of the transcription termination factor Rho causes pervasive transcription and rapid death. *Nat. Commun* **8**, 1–10
15. Bidnenko, V., Nicolas, P., Grylak-Mielnicka, A., Delumeau, O., Auger, S., Aucouturier, A., *et al.* (2017) Termination factor Rho: from the control

of pervasive transcription to cell fate determination in Bacillus subtilis. *PLoS Genet.* **13**, e1006909
16. Bidnenko, V., Nicolas, P., Guérin, C., Dérozier, S., Chastanet, A., Dairou, J., *et al.* (2023) Termination factor Rho mediates transcriptional reprogramming of Bacillus subtilis stationary phase. *PLoS Genet.* **19**, e1010618
17. Nagel, A., Michalik, S., Debarbouille, M., Hertlein, T., Gesell Salazar, M., Rath, H., *et al.* (2018) Inhibition of rho activity increases expression of SaeRS-dependent virulence factor genes in Staphylococcus aureus, showing a link between transcription termination, antibiotic action, and virulence. *MBio* **9**, e01332-18
18. Trzilova, D., Anjuwon-Foster, B. R., Torres Rivera, D., and Tamayo, R. (2020) Rho factor mediates flagellum and toxin phase variation and impacts virulence in Clostridioides difficile. *PLoS Pathog.* **16**, e1008708
19. Lin, Y., Alstrup, M., Pang, J. K. Y., Maróti, G., Er-Rafik, M., Tourasse, N., *et al.* (2021) Adaptation of Bacillus thuringiensis to plant colonization affects differentiation and toxicity. *Msystems* **6**, e00864-21
20. Krypotou, E., Townsend, G. E., Gao, X., Tachiyama, S., Liu, J., Pokorzynski, N. D., *et al.* (2023) Bacteria require phase separation for fitness in the mammalian gut. *Science* **379**, 1149–1156
21. Lee, Y. H., and Helmann, J. D. (2014) Mutations in the primary sigma factor σa and termination factor rho that reduce susceptibility to cell wall antibiotics. *J. Bacteriol.* **196**, 3700–3711
22. Liu, B., Kearns, D. B., and Bechhofer, D. H. (2016) Expression of multiple Bacillus subtilis genes is controlled by decay of slrA mRNA from Rho dependent 3' ends. *Nucleic Acids Res.* **44**, 3364–3372
23. Hafeezunnisa, M., and Sen, R. (2020) The Rho-dependent transcription termination is involved in broad-spectrum antibiotic susceptibility in Escherichia coli. *Front. Microbiol.* **11**, 3059
24. Figueroa-Bossi, N., Sánchez-Romero, M. A., Kerboriou, P., Naquin, D., Bossi, L., Bouloc, P., *et al.* (2022) Pervasive transcription enhances the accessibility of H-NS–silenced promoters and generates bistability in Salmonella virulence gene expression. *Proc. Natl. Acad. Sci. U. S. A.* **119**, e2203011119
25. Pérez-Varela, M., Singh, R., Colquhoun, J. M., Starich, O. G., Tierney, A. R. P., Tipton, K. A., *et al.* (2024) Evidence for Rho-dependent control of a virulence switch in Acinetobacter baumannii. *mBio* **15**, e02708-23
26. de Hoon, M. J., Eichenberger, P., and Vitkup, D. (2010) Hierarchical evolution of the bacterial sporulation network. *Curr. Biol.* **20**, R735–R745
27. Swick, M. C., Koehler, T. M., and Driks, A. (2016) Surviving between hosts: sporulation and transmission. *Microbiol. Spectr.* **4**, 10
28. Galperin, M. Y., Yutin, N., Wolf, Y. I., Vera Alvarez, R., and Koonin, E. V. (2022) Conservation and evolution of the sporulation gene set in diverse members of the firmicutes. *J. Bacteriol.* **21**, e0007922
29. Setlow, P. (2003) Spore germination. *Curr. Opin. Microbiol.* **6**, 550–556
30. Setlow, P., Wang, S., and Li, Y. Q. (2017) Germination of spores of the orders bacillales and clostridiales. *Annu. Rev. Microbiol.* **71**, 459–477
31. Setlow, P., and Christie, G. (2023) New Thoughts on an Old Topic: secrets of bacterial spore resistance slowly being revealed. *Microbiol. Mol. Biol. Rev.* **87**, e00080-22
32. Segev, E., Rosenberg, A., Mamou, G., Sinai, L., and Ben-Yehuda, S. (2013) Molecular kinetics of reviving bacterial spores. *J. Bacteriol.* **195**, 1875–1882
33. Abhyankar, W. R., Kamphorst, K., Swarge, B. N., Van Veen, H., De Koning, L. J., Brul, S., *et al.* (2016) The influence of sporulation conditions on the spore coat protein composition of Bacillus subtilis spores. *Front. Microbiol.* **7**, 1636
34. Mutlu, A., Trauth, S., Ziesack, M., Nagler, K., Bischofs, I. B., Rohr, K., *et al.* (2018) Phenotypic memory in Bacillus subtilis links dormancy entry and exit by a spore quantity-quality tradeoff. *Nat. Commun.* **9**, 69
35. Mutlu, A., Kaspar, C., Becker, N., and Bischofs, I. B. (2020) A spore quality–quantity tradeoff favors diverse sporulation strategies in Bacillus subtilis. *ISME J.* **14**, 2703–2714
36. Londono-Vallejo, J. A., and Stragier, P. (1995) Cell-cell signaling pathway activating a developmental transcription factor in Bacillus subtilis. *Genes Dev.* **9**, 503–508
37. Errington, J. (1993) Bacillus subtilis sporulation: regulation of gene expression and control of morphogenesis. *Microbiol. Rev.* **57**, 1–33
38. Stragier, P., and Losick, R. (1996) Molecular genetics of sporulation in Bacillus subtilis. *Annu. Rev. Genet.* **30**, 297
39. Piggot, P. J., and Hilbert, D. W. (2004) Sporulation of Bacillus subtilis. *Curr. Opin. Microbiol.* **7**, 579–586
40. Higgins, D., and Dworkin, J. (2012) Recent progress in *Bacillus subtilis* sporulation. *FEMS Microbiol. Rev.* **36**, 131–148
41. Eichenberger, P., Jensen, S. T., Conlon, E. M., van Ooij, C., Silvaggi, J., González-Pastor, J. E., *et al.* (2003) The σE regulon and the identification of additional sporulation genes in Bacillus subtilis. *J. Mol. Biol.* **327**, 945–972
42. Eichenberger, P., Fujita, M., Jensen, S. T., Conlon, E. M., Rudner, D. Z., Wang, S. T., *et al.* (2004) The program of gene transcription for a single differentiating cell type during sporulation in Bacillus subtilis. *PLoS Biol.* **2**, e328
43. Steil, L., Serrano, M., Henriques, A. O., and Völker, U. (2005) Genome-wide analysis of temporally regulated and compartment-specific gene expression in sporulating cells of Bacillus subtilis. *Microbiol* **151**, 399–420
44. Wang, S. T., Setlow, B., Conlon, E. M., Lyon, J. L., Imamura, D., Sato, T., *et al.* (2006) The forespore line of gene expression in Bacillus subtilis. *J. Mol. Biol.* **21**, 16–37
45. Overkamp, W., and Kuipers, O. P. (2015) Transcriptional profile of Bacillus subtilis sigF-mutant during vegetative growth. *PLoS One* **27**, e0141553
46. Meeske, A. J., Rodrigues, C. D., Brady, J., Lim, H. C., Bernhardt, T. G., and Rudner, D. Z. (2016) High-throughput genetic screens identify a large and diverse collection of new sporulation genes in Bacillus subtilis. *PLoS Biol.* **14**, e1002341
47. Ingham, C. J., Dennis, J., and Furneaux, P. A. (1999) Autogenous regulation of transcription termination factor Rho and the requirement for Nus factors in Bacillus subtilis. *Mol. Microbiol.* **31**, 651–663
48. Barik, S., Bhattacharya, P., and Das, A. (1985) Autogenous regulation of transcription termination factor Rho. *J. Mol. Biol.* **182**, 495–508
49. Matsumoto, Y., Shigesada, K., Hirano, M., and Imai, M. (1986) Autogenous regulation of the gene for transcription termination factor rho in Escherichia coli: localization and function of its attenuators. *J. Bacteriol.* **166**, 945–958
50. Italiani, V. C., and Marques, M. V. (2005) The transcription termination factor Rho is essential and autoregulated in Caulobacter crescentus. *J. Bacteriol.* **187**, 4290–4294
51. Silva, I. J., Barahona, S., Eyraud, A., Lalaouna, D., Figueroa-Bossi, N., Massé, E., and Arraiano, C. M. (2019) SraL sRNA interaction regulates the terminator by preventing premature transcription termination of rho mRNA. *Proc. Natl. Acad. Sci. U. S. A.* **116**, 3042–3051
52. Mirouze, N., Desai, Y., Raj, A., and Dubnau, D. (2012) Spo0A∼P imposes a temporal gate for the bimodal expression of competence in Bacillus subtilis. *PLoS Genet.* **8**, e1002586
53. Lewandoski, M., Dubnau, E., and Smith, I. (1986) Transcriptional regulation of the spo0F gene of Bacillus subtilis. *J. Bacteriol.* **168**, 870–877
54. Predich, M., Nair, G., and Smith, I. (1992) Bacillus subtilis early sporulation genes kinA, spo0F, and spo0A are transcribed by the RNA polymerase containing sigma H. *J. Bacteriol.* **174**, 2771–2778
55. Strauch, M. A., Wu, J.-J., Jonas, R. H., and Hoch, J. A. (1993) A positive feedback loop controls transcription of the spo0F gene, a component of the sporulation phosphorelay in Bacillus subtilis. *Mol. Microbiol.* **7**, 967–974
56. Asayama, M., Yamamoto, A., and Kobayashi, Y. (1995) Dimer form of phosphorylated Spo0A, a transcriptional regulator, stimulates the spo0F transcription at the initiation of sporulation in Bacillus subtilis. *J. Mol. Biol.* **250**, 11–23
57. Vagner, V., Dervyn, E., and Ehrlich, S. D. (1998) A vector for systematic gene inactivation in Bacillus subtilis. *Microbiol* **144**, 3097–3104
58. Illing, N., and Errington, J. (1991) Genetic regulation of morphogenesis in Bacillus subtilis: roles of sigma E and sigma F in prespore engulfment. *J. Bacteriol.* **173**, 3159–3169

59. Setlow, B., Magill, N., Febbroriello, P., Nakhimovsky, L., Koppel, D. E., and Setlow, P. (1991) Condensation of the forespore nucleoid early in sporulation of Bacillus species. *J. Bacteriol.* **173**, 6270–6278
60. Lewis, P. J., Partridge, S. R., and Errington, J. (1994) Sigma factors, asymmetry, and the determination of cell fate in Bacillus subtilis. *Proc. Natl. Acad. Sci. U. S. A.* **91**, 3849–3853
61. Eichenberger, P., Fawcett, P., and Losick, R. (2001) A three-protein inhibitor of polar septation during sporulation in Bacillus subtilis. *Mol. Microbiol.* **42**, 1147–1162
62. Amaya, E., Khvorova, A., and Piggot, P. J. (2001) Analysis of promoter recognition in vivo directed by ςF of Bacillus subtilis by using random-sequence oligonucleotides. *J. Bacteriol.* **183**, 3623–3630
63. Setlow, P. (2006) Spores of Bacillus subtilis: their resistance to and killing by radiation, heat and chemicals. *J. Appl. Microbiol.* **101**, 514–525
64. Henriques, A. O., and Moran Jr, C. P. (2007) Structure, assembly, and function of the spore surface layers. *Annu. Rev. Microbiol.* **61**, 555–588
65. Nicholson, W. L., Munakata, N., Horneck, G., Melosh, H. J., and Setlow, P. (2000) Resistance of Bacillus endospores to extreme terrestrial and extraterrestrial environments. *Microbiol. Mol. Biol. Rev.* **64**, 548–572
66. Setlow, P. (2016) Spore resistance properties. The bacterial spore: from molecules to systems. *Microbiol. Spectr.* **2**, 201–215
67. McKenney, P. T., Driks, A., and Eichenberger, P. (2013) The Bacillus subtilis endospore: assembly and functions of the multilayered coat. *Nat. Rev. Microbiol* **11**, 33–44
68. Driks, A., and Eichenberger, P. (2016) The spore coat. The bacterial spore: from molecules to systems. *Microbiol. Spectr.* **4**, 179–200
69. Setlow, P. (2013) Summer meeting 2013–when the sleepers wake: the germination of spores of Bacillus species. *J. Appl. Microbiol.* **115**, 1251–1268
70. Sinai, L., Rosenberg, A., Smith, Y., Segev, E., and Ben-Yehuda, S. (2015) The molecular timeline of a reviving bacterial spore. *Mol. Cell* **57**, 695–707
71. Ramírez-Guadiana, F. H., Meeske, A. J., Wang, X., Rodrigues, C. D. A., and Rudner, D. Z. (2017) The Bacillus subtilis germinant receptor GerA triggers premature germination in response to morphological defects during sporulation. *Mol. Microbiol.* **105**, 689–704
72. Christie, G., and Setlow, P. (2020) Bacillus spore germination: knowns, unknowns and what we need to learn. *Cell Signal.* **74**, 109729
73. Rosenberg, A., Soufi, B., Ravikumar, V., Soares, N. C., Krug, K., Smith, Y., *et al.* (2015) Phosphoproteome dynamics mediate revival of bacterial spores. *BMC Biol.* **13**, 1–19
74. Chastanet, A., Vitkup, D., Yuan, G. C., Norman, T. M., Liu, J. S., and Losick, R. M. (2010) Broadly heterogeneous activation of the master regulator for sporulation in Bacillus subtilis. *Proc. Natl. Acad. Sci. U. S. A.* **107**, 8486–8491
75. Fujita, M., and Losick, R. (2009) The master regulator for entry into sporulation in Bacillus subtilis becomes a cell-specific transcription factor after asymmetric division. *Genes Dev.* **17**, 1166–1174
76. Mason, J. M., and Setlow, P. (1986) Essential role of small, acid-soluble spore proteins in resistance of Bacillus subtilis spores to UV light. *J. Bacteriol.* **167**, 174–178
77. Pedraza-Reyes, M., Gutiérrez-Corona, F., and Nicholson, W. L. (1994) Temporal regulation and forespore-specific expression of the spore photoproduct lyase gene by sigma-G RNA polymerase during Bacillus subtilis sporulation. *J. Bacteriol.* **176**, 3983–3991
78. Setlow, P. I. (2007) Will survive: DNA protection in bacterial spores. *Trends Microbiol.* **15**, 172–180
79. Swarge, B., Abhyankar, W., Jonker, M., Hoefsloot, H., Kramer, G., Setlow, P., *et al.* (2020) Integrative analysis of proteome and transcriptome dynamics during Bacillus subtilis spore revival. *mSphere* **5**, e00463-20
80. Tu, Z., Dekker, H. L., Roseboom, W., Swarge, B. N., Setlow, P., Brul, S., and Kramer, G. (2021) High resolution analysis of proteome dynamics during *Bacillus subtilis* sporulation. *Int. J. Mol. Sci.* **22**, 9345
81. Dérozier, S., Nicolas, P., Mäder, U., and Guérin, C. (2021) Genoscapist: online exploration of quantitative profiles along genomes via interactively customized graphical representations. *Bioinformatics* **37**, 2747–2749
82. McPherson, D. C., Kim, H., Hahn, M., Wang, R., Grabowski, P., Eichenberger, P., *et al.* (2005) Characterization of the Bacillus subtilis spore morphogenetic coat protein CotO. *J. Bacteriol.* **187**, 8278–8290
83. Zilhão, R., Naclerio, G., Henriques, A. O., Baccigalupi, L., Moran, C. P., Jr., and Ricca, E. (1999) Assembly requirements and role of CotH during spore coat formation in Bacillus subtilis. *J. Bacteriol.* **181**, 2631–2633
84. Isticato, R., Lanzilli, M., Petrillo, C., Donadio, G., Baccigalupi, L., and Ricca, E. (2020) Bacillus subtilis builds structurally and functionally different spores in response to the temperature of growth. *Environ. Microbiol.* **22**, 170–182
85. Freitas, C., Plannic, J., Isticato, R., Henriques, A. O., Zilhão, R., Serrano, M., *et al.* (2020) A protein phosphorylation module patterns the Bacillus subtilis spore outer coat. *Mol. Microbiol.* **114**, 934–951
86. Henriques, A. O., Melsen, L. R., and Moran, C. P., Jr. (1998) Involvement of superoxide dismutase in spore coat assembly in Bacillus subtilis. *J. Bacteriol.* **180**, 2285–2291
87. Real, G., Pinto, S. M., Schyns, G., Costa, T., Henriques, A. O., and Moran, C. P., Jr. (2005) A gene encoding a holin-like protein involved in spore morphogenesis and spore germination in Bacillus subtilis. *J. Bacteriol.* **187**, 6443–6453
88. Nguyen, K. B., Sreelatha, A., Durrant, E. S., Lopez-Garrido, J., Muszewska, A., Tagliabracci, V. S., *et al.* (2016) Phosphorylation of spore coat proteins by a family of atypical protein kinases. *Proc. Natl. Acad. Sci. U. S. A.* **113**, E3482–E3491
89. Di Gregorio Barletta, G., Vittoria, M., Lanzilli, M., Petrillo, C., Ricca, E., and Isticato, R. (2022) CotG controls spore surface formation in response to the temperature of growth in Bacillus subtilis. *Environ. Microbiol.* **24**, 2078–2088
90. Cabrera-Martinez, R. M., Tovar-Rojo, F., Vepachedu, V. R., and Setlow, P. (2003) Effects of overexpression of nutrient receptors on germination of spores of Bacillus subtilis. *J. Bacteriol.* **185**, 2457–2464
91. Ghosh, S., Scotland, M., and Setlow, P. (2012) Levels of germination proteins in dormant and superdormant spores of Bacillus subtilis. *J. Bacteriol.* **194**, 2221–2227
92. Chen, Y., Ray, W. K., Helm, R. F., Melville, S. B., and Popham, D. L. (2014) Levels of germination proteins in Bacillus subtilis dormant, superdormant, and germinating spores. *PLoS One* **9**, e95781
93. Corfe, B. M., Sammons, R. L., Smith, D. A., and Mauël, C. (1994) The gerB region of the Bacillus subtilis 168 chromosome encodes a homologue of the gerA spore germination operon. *Microbiol.* **140**, 471–478
94. Feavers, I. M., Foulkes, J., Setlow, B., Sun, D., Nicholson, W., Setlow, P., *et al.* (1990) The regulation of transcription of the *gerA* spore germination operon of *Bacillus subtilis*. *Mol. Microbiol.* **4**, 275–282
95. Amon, J. D., Artzi, L., and Rudner, D. Z. (2022) Genetic evidence for signal transduction within the *Bacillus subtilis* GerA germinant receptor. *J. Bacteriol.* **204**, e0047021
96. Paidhungat, M., and Setlow, P. (2000) Role of Ger proteins in nutrient and nonnutrient triggering of spore germination in Bacillus subtilis. *J. Bacteriol.* **182**, 2513–2519
97. Paidhungat, M., Ragkousi, K., and Setlow, P. (2001) Genetic requirements for induction of germination of spores of Bacillus subtilis by Ca(2+)-dipicolinate. *J. Bacteriol.* **183**, 4886–4893
98. Segev, E., Smith, Y., and Ben-Yehuda, S. (2012) RNA dynamics in aging bacterial spores. *Cell* **148**, 139–149
99. Bressuire-Isoard, C., Broussolle, V., and Carlin, F. (2018) Sporulation environment influences spore properties in Bacillus: evidence and insights on underlying molecular and physiological mechanisms. *FEMS Microbiol. Rev.* **42**, 614–626
100. Rao, L., Zhou, B., Serruya, R., Moussaieff, A., Sinai, L., and Ben-Yehuda, S. (2022) Glutamate catabolism during sporulation determines the success of the future spore germination. *iScience* **25**, 105242
101. O'Brien, T., and Campbell, Jr L. L. (1957) The nutritional requirements for germination and out-growth of spores and vegetative cell growth of some aerobic spore forming bacteria. *J. Bacteriol.* **73**, 522–525
102. Harwood, C. R., and Cutting, S. M. (1990) *Molecular Biological Methods for bacillus.* John Wiley, Chichester, NY

103. Schaeffer, P., Millet, J., and Aubert, J.-P. (1965) Catabolic repression of bacterial sporulation. *Proc. Natl. Acad. Sci. U. S. A.* **54**, 704–711
104. Arnaud, M., Chastanet, A., and Débarbouillé, M. (2004) New vector for efficient allelic replacement in naturally nontransformable, low-GC-content, gram-positive bacteria. *Appl. Environ. Microbiol.* **70**, 6887–6891
105. van Ooij, C., Eichenberger, P., and Losick, R. (2004) Dynamic patterns of subcellular protein localization during spore coat morphogenesis in Bacillus subtilis. *J. Bacteriol.* **186**, 4441–4448
106. Schindelin, J., Arganda-Carreras, I., Frise, E., Kaynig, V., Longair, M., Pietzsch, T., *et al.* (2012) Fiji: an open-source platform for biological-image analysis. *Nat. Methods* **9**, 676–682
107. Bechhofer, D. H., Oussenko, I. A., Deikus, G., Yao, S., Mathy, N., and Condon, C. (2008) Analysis of mRNA decay in Bacillus subtilis. *Methods Enzymol.* **447**, 259–276
108. Redko, Y., Aubert, S., Stachowicz, A., Lenormand, P., Namane, A., Darfeuille, F., *et al.* (2013) A minimal bacterial RNase J-based degradosome is associated with translating ribosomes. *Nucleic Acids Res.* **41**, 288–301
109. Gilet, L., Pellegrini, O., Trinquier, A., Tolcan, A., Allouche, D., *et al.* (2020) Analysis of Bacillus subtilis ribonuclease activity in vivo. In *RNA Remodeling Proteins: Methods and Protocols*. Springer US, New York, NY
110. Riesenman, P. J., and Nicholson, W. L. (2000) Role of the spore coat layers in Bacillus subtilis spore resistance to hydrogen peroxide, artificial UV-C, UV-B, and solar UV radiation. *Appl. Environ. Microbiol.* **66**, 620–626
111. Theodorou, I., Courtin, P., Palussière, S., Kulakauskas, S., Bidnenko, E., Péchoux, C., *et al.* (2019) A dual-chain assembly pathway generates the high structural diversity of cell-wall polysaccharides in Lactococcus lactis. *J. Biol. Chem.* **294**, 17612–17625
112. Koo, B. M., Kritikos, G., Farelli, J. D., Todor, H., Tong, K., Kimsey, H., *et al.* (2017) Construction and analysis of two genome-scale deletion libraries for Bacillus subtilis. *Cell Syst.* **4**, 291–305
113. Fawcett, P., Eichenberger, P., Losick, R., and Youngman, P. (2000) The transcriptional profile of early to middle sporulation in Bacillus subtilis. *Proc. Natl. Acad. Sci. U. S. A.* **97**, 8063–8068
114. Kenney, T. J., and Moran, Jr C. P. (1987) Organization and regulation of an operon that encodes a sporulation-essential sigma factor in Bacillus subtilis. *J. Bacteriol.* **169**, 3329–3339
115. Guérout-Fleury, A. M., Frandsen, N., and Stragier, P. (1996) Plasmids for ectopic integration in Bacillus subtilis. *Gene* **180**, 57–61
116. Mirouze, N., Prepiak, P., and Dubnau, D. (2011) Fluctuations in spo0A transcription control rare developmental transitions in Bacillus subtilis. *PLoS Genet.* **7**, e1002048